
Dear Editor and reviewers,

Thank you for your attention. We appreciate your earnest work including comments and suggestions concerning our manuscript. Based on the comments, we have made careful modifications on the original manuscript. As required by this journal, the responses to the referees have been structured as follows: (1) comments from Referees and corresponding author's response, and (2) author's changes in manuscript. Therefore, we have responded to the reviewers in the sequence: (1) the original comments (from each reviewer) in black and our point-by-point responses in blue, and (2) our revised manuscript highlighted using “track change”. All line numbers in the responses are made with respect to this “track change” version of the manuscript.

The details of the response to the two referees and the corresponding revised manuscript are shown in the following section. We hope that the revised manuscript at this stage could be qualified for potential publication, and we look forward to hearing from you soon.

Yours sincerely,

Prof. Yongqiang Zhang; Dr. Peilin Song

Key Laboratory of Water Cycle and Related Land Surface Processes, Institute of Geographic Sciences and Natural Resources Research, The Chinese Academy of Sciences, Beijing 100101, China

Emails: zhangyq@igsnr.ac.cn; songpl@igsnr.ac.cn

Author Response to RC1

Journal: ESSD

Title: A 1-km daily surface soil moisture dataset of enhanced coverage under all-weather conditions over China in 2003-2019

Author(s): Peilin Song et al.

MS No.: essd-2021-428

MS Type: Data description paper

General Comments:

“This paper proposes fine-resolution surface soil moisture (SSM) data over China. The significance and potential impact are clear, and the novelty and results are promising. However, a major revision is needed to address my concerns.”

Response:

All authors greatly appreciate you for your constructive comments that have helped improve our paper. We have paid great attentions on each bullet pointed out by you and have modified our paper carefully based on your comments. Please see the following responses to your specific comments and technical comments.

Response to specific comments

1) *“Line 236: About the LST validation:*

Aqua nighttime passing time can be 1-hour away from 1:30 am LT. Even nighttime LST does have small variations than daytime LST, can you find some sites with minute-level observations in China to prove that using ground observations at 2:00 am introduces little uncertainty to the validation results?

Besides, the 0-cm ground temperature is different from LST physically, especially over vegetated areas, where SSM estimation by LST may have considerable uncertainty. Over these places, LST is closer to vegetation canopy temperature (air temperature). To address my two concerns above, I would recommend including a brief test in the discussion by using site-measured LSTs that are computed by surface upward longwave radiation and BBE, and it would be convincing to include sites over various land cover types.”

Response:

Thanks for your suggestion. We have added a new Section 4.2 to discuss this question as well as your Questions 3 and 5 below. For the current discussion, please see Lines 669-686 for details. Basically, we cannot use flux towers to substitute validation data derived at meteorological stations because the spatial density and temporal coverage of the former dataset are not adequately high to represent the entire China. However, following your suggestion, we have implemented the test to address these two concerns in the added Section Appendix C.

In Appendix C, we selected 4 extra flux towers where long radiation observations are publicly available for a comparison with our 0-cm ground temperature, based on your suggestion. The minute-level LST of these towers between 1:00-2:00 A.M. are stable and consistent with the night-time 0-cm ground temperature at meteorological stations.

But one point we need to stress is that the meteorological sites are all located “under open environmental conditions with relatively lower fraction of tall trees and water bodies”(see Lines 677-679 in Section 4.2), according to the official regulation of the National Meteorological Administration of China. Also, it is difficult to find flux towers paired with meteorological stations over densely vegetated regions. Instead, the 4 towers are all located within grasslands across the country.

Besides, we have also re-checked the overpass time of MODIS LST product. The extreme time deviation from 1:30 A.M. can be about 15-20 minutes in our study period and region, not as large as one hour.

2) *“is there any evidence to prove the rationality of ‘7x7’ and ‘-5_{th} to 5_{th}’?”*

Response:

These two values have been actually determined as the optimal ones based on our test and evaluation against in-situ data from a collection of values. We have revised the paper by adding this description. Please see Lines 360-368.

3) *“Fig 3: Clear bias is still shown in filled LST results (Fig 3b) compared to the clear-sky validation (Fig 3a). Will it affect the SSM estimation when clear-sky (unbiased) and filled LSTs (biased) simultaneously exist in a spatial window using the ‘universal triangle feature’ or in SEE calculation?”*

Response:

Thanks for this comment. There is indeed inevitable influence for such clear-sky-to-cloud mixed windows when we intend for a dataset of quasi-complete coverage. Based on your question, we have added a brief discussion on this in the new added Section 4.2. Please see Lines 657-668.

In summary, such influence implies that the actual difference between SSM downscaling results at cloudy and at clear-sky conditions may be larger than “0.056 vol/vol VS 0.053 vol/vol”. But overall, it should not affect the main features of the proposed product (e.g. the better performance of the STDF-derived LST in downscaling cloudy SSM compared to the bias-adjusted one). Also, such possible sacrifice for accuracy of clear-sky SSM in the clear-sky-to-cloud mixed windows can make the product accuracy more consistent between cloudy

and clear-sky conditions. This is beneficial to wider application of the product in future studies.

4.1) “Fig 5: After readers notice the clear differences between two data at some locations (Fig 5a&b), they may want to know which data is more accurate.

In order to address this concern, you may need to focus on the sites over these regions, where the proposed data have considerable differences with SMAP-Sentinel (e.g. far northeastern, northern west, southern provinces near the sea), specifically and separately, rather than just over entire China (Line 499). ”

Response:

We had actually carried out such analysis which is consistent with your suggestion. In this regard, we produced a map for demonstrating all available validation sites in terms of the direct ubRMSD difference (at each site) based on ubRMSD of SMAP-sentinel data minus that of the proposed product. From the map (see the Fig.1 below), however, we cannot find significantly different regional (e.g. between the northeast and the southwest) patterns of the “ubRMSD difference”. As a consequence, we decided to maintain the current validation strategy for our paper. Detailed reasons are as follows:

(1) First, from the map below we can see that the validation sites are not evenly distributed across the country, especially considering the much smaller number of sites in the southwestern part. This makes it difficult to make a fair comparison for different sub-regions.

(2) Second, it is important to notice that validation of remote sensing soil moisture based on site measurements actually evaluates the similarity of the “trends” in both the spatial and the temporal dimensions between remote sensing and in situ data. But for the sub-regional validation, we can only evaluate the site-based temporal trend or spatial trend at a much smaller spatio scale but have to abandon the national-scale spatial trend which is especially important. This indicates that the overall validation across the country can be a more comprehensive and more fair validation strategy.

(3) The main object of our paper is to develop a product of higher temporal resolution, higher coverage and higher accuracy than current data (SMAP-Sentinel). As with comparing the detailed qualities of different data products in different sub-regions, the map (in Fig.1 below) indicates that the inconsistent performances of the products cannot be simply ascribed to their differences on geographical locations or climatic regions. In reality, as the basic theories, data inputs, mathematical algorithms, and uncertainty sources differ completely between SMAP-Sentinel combined and PM-optical-data combined downscaling frameworks, the complexity of this issue may be beyond the center topic of current study and need to be investigated specifically in the future.

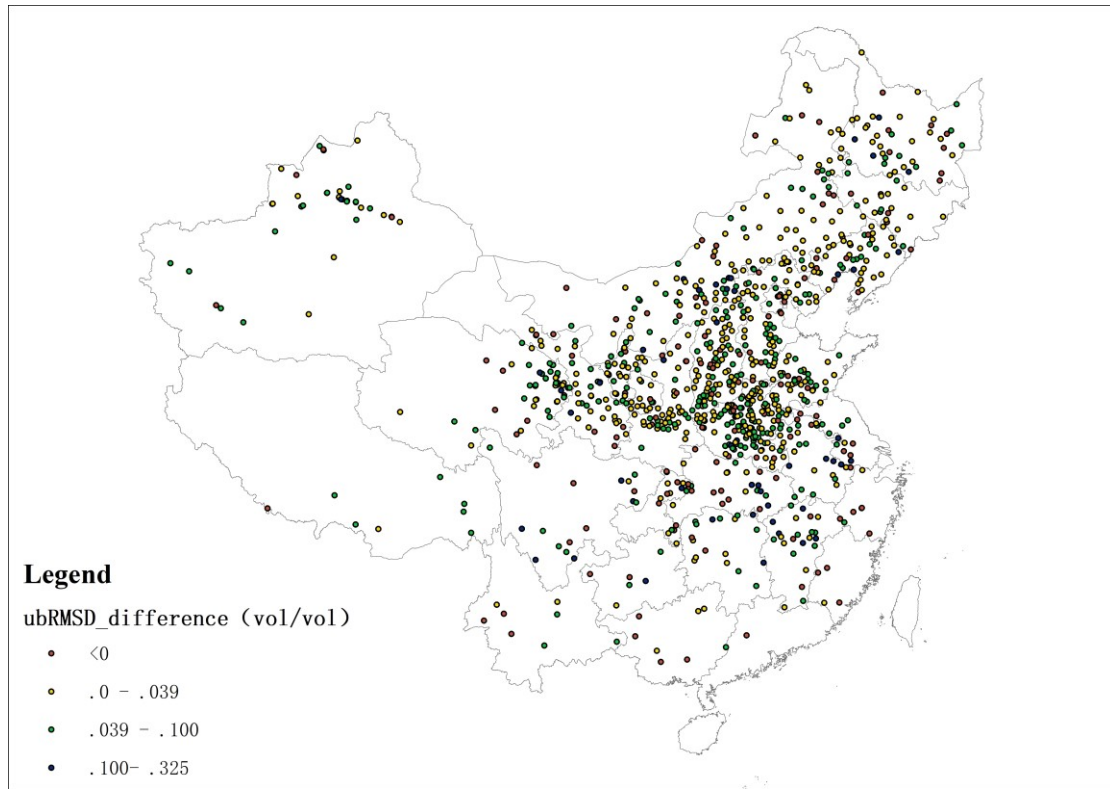


Fig. 1 The spatial distribution for Difference of single-site-based ubRMSD of SMAP-sentinel data minus that of our proposed product ($\text{ubRMSD}_{\text{sentinel-smap}} - \text{ubRMSD}_{\text{proposed}}$), corresponding to Fig.5 in the paper. Sites with samples less than 20 for one year are excluded.

4.2) “Besides, SMAP shows a very good accuracy (Fig A1a) while the downscaled SMAP-Sentinel (Fig 5c) has large (nearly doubled) ubRMSD. Can you explain why the accuracy is considerably decreased after downscaling?”

Response:

According to the authors of the SMAP-Sentinel product (Das et al., 2019), uncertainty of this product includes that from its ancillary datasets, the optimization process on its model coefficients, as well as the increased speckle noise introduced when the spatial resolution of Sentinel-1 data is enhanced from 9 km to 1 km. Therefore, the authors of Das et al. (2019) comment that there is “tradeoff between adding spatial resolution with C-band SAR data and noise-levels”. This can explain why SMAP-Sentinel has larger ubRMSD than SMAP data. This result is also supported by another previous evaluation study (Mohammad et al., 2018).

On the other hand, we understand that you may have concern on the result that the SMAP-Sentinel based ubRMSD is nearly doubled after downscaled. However, it is important to notice that the analyses in Appendix A and in Fig.5 are not based on the same numbers of validation sites. In Appendix A we only employed quite a small portion of the sites in only 53 microwave 36-km grids because only these sites have the qualified distribution density for representing the microwave grids. As these sites are mostly distributed in plain regions (see Fig. A1), there is a chance to further enlarge its performance difference with the SMAP-Sentinel based result because the latter is evaluated based on a much larger number of validation sites. As a conclusion, we can compare the performance difference between SMAP-Sentinel and our proposed data in Fig.5 as they are based on the equivalent sampling size, whilst it is more or less not fair to quantitatively analyze the decreased ubRMSD of

SMAP-Sentinel data against that of SMAP data between Fig.5 and Fig.A1.

5)“Appendix B: It’s strange that filled LST with considerable bias (-1.7 K) can achieve better SSM accuracy (0.058 vol/vol) than the SSM (0.064 vol/vol) from more accurate/realistic cloudy-sky LST in Fig. A3, and such accuracy difference is even larger than its difference with the clear-sky SSM (0.053 vol/vol, LST is unbiased). If that is the case, the logic behind it is that SSM is not sensitive to the LST, which is not right.

Besides, the LST bias explanation in Lines 309-311 is not convincing: if the filled LST has clear bias compared to site observations, it only means it cannot reflect the realistic surface condition.”

Response:

We basically accept your comment that Lines 309-311 is not convincing enough. Now we have modified and moved these sentences to Lines 634-668 in the new added Section 4.2 as a better and more open discussion. In brief, the STDF-derived LST under cloud with clear bias may not be suitable for all cloudy conditions, especially we agree with you that it is not suitable for rainy cloud. However, we argue that it can explain at least a substantial part of the non-rainy cloud condition. For the bias-adjusted cloud gap-filled LST, although it is better in reflecting the realistic surface condition, such mechanical relationships among cloud, LST and SSM can be beyond what has been described by the UTFS theory which was originally proposed for clear sky only (see the Fig.2 below for illustration).

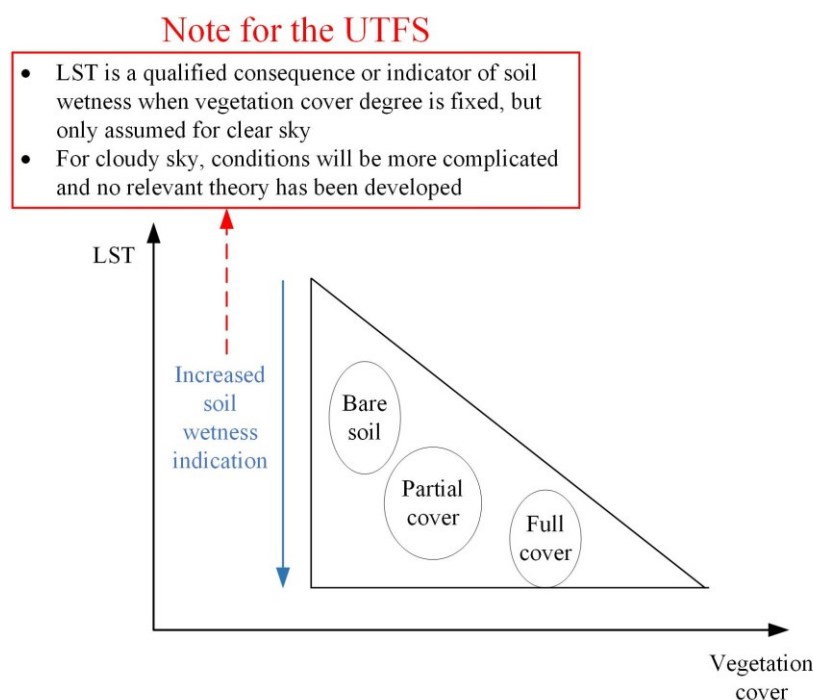


Fig.2 Illustration of the UTFS theory under clear sky

In our revised discussion, therefore, the higher ubRMSD of STDF-derived LST compared to real clear-sky data (0.056 vol/vol VS 0.053 vol/vol) suggests such a gap-filling strategy (based on STDF alone) is not 100% perfect (especially for rainy weather which is the most difficult for the entire community of land surface remote sensing) and further improvements

are encouraged, whilst the even higher ubRMSD of non-bias or bias-adjusted LST under cloud (0.064 vol/vol) suggests that the STDF-derived LST is at least a better alternative compared to its bias-adjusted counterpart.

Meanwhile, we also need to stress that the results in Appendix B do not indicate “SSM is not sensitive to LST”, because if it is not sensitive, all three groups of SSM should not have difference in their validation performance. The results just indicate the difference of “LST-SSM” interaction mechanisms between clear-sky and cloudy conditions.

Response to technical comments

Comments	Response
Lines 50-56: references are necessary for the background knowledge introduction, especially for the potential application examples	Accepted. See the revised beginning of the Introduction. (Lines 54-58)
Line 87: “universal triangle feature (UTF)” or “triangle feature space (TFS)”?	Accepted. We revised and unified the term as “universal triangle feature space (UTFS)” through the text.
Line 91: please define the acronym UCLA	Done as suggested. (Line 93)
Line 109: ‘,’ should be removed	Done as suggested.
Lines 78-80, 112-113: references, please.	For Lines 78-80, we have accepted your advice and added references. For Line 112-113, “the above-mentioned optical/infrared-data-based downscaling methods” have had their references listed above when each method was firstly described. So there is no need to repeat here.
Line 117: ‘whilst .. even inferior’ is not appropriate here. There is no such logic in the context unless you mean ‘UTF-based methods are found even inferior to the DISPATCH in a typical humid region’	We have altered it to another formulation that weakens such a logic. See Lines 120-122 (“ <i>As far as the UTFS-based method is concerned, a poorer performance was obtained compared to the DISPATCH in a typical water-limited region in North America</i> ”). The main idea we intend to convey is that universality for both of the methods is not perfect enough currently.
Lines 124: the objectives you mentioned here are more like broad impacts or potential significance while the objective of a study should be specific.	Accepted. We have changed the term as “potential significance”, because the objective has been described just in the current paragraph (to produce the data product, Lines 123-127)
Line 144: ‘after’ or ‘in the’?	Accepted. Changed to “in the”.
Lines 179, 360: ‘high resolution’ -> ‘fine-	Done as suggested.

resolution'	
Table 1: url -> URL	Done as suggested.
Line 196: 'be' -> 'being'	Done as suggested.
Line 205: 'the'	Accepted and removed.
Lines 217-232: Please also include some literature to prove that these involved sites are spatially representative at km scales or have been widely used in SSM validation.	Accepted. Please see Lines 231-232 for the added literatures showing it has been widely used.
Line 224: '2014)'	Done as suggested.
Line 262: is the '10-cm-depth' different from the '0-10 cm' like you mentioned in Line 229?	Accepted. They are the same in effect. We have revised the former as "0-10 cm".
Line 285: Do you mean that one set of coefficients a-d will be used for all pixels of the whole country on t1?	Yes. We have actually tested different solutions including sub-region-based coefficients and the common set of coefficients for all of the country. The data outcome based the common set of coefficients for a certain date has the best quality (obtaining both high accuracy and high coverage).
Lines 309-311: I agree that STDF is enough for the accuracy requirement of soil moisture estimation. However, this explanation here is weird because the atmosphere does have interactions with the surface at cloudy-sky: cloudy conditions may also indicate it is raining or the atmosphere is wet. Such LST and ET disturbance signals, which can be captured by PM-based LST but not by STDF, will impact the soil moisture. In other words, the atmospheric condition cannot be simply separated by using such an explanation.	We appreciate your agreement on our methodology. For the discussion, you can see our detailed response to your Specific Comment 5 above. Basically, we agree with you that atmospheric condition can bring extra uncertainty when we use STDF-derived LST as input, and we have better discussed it in the new added Section 4.2. However, this uncertainty can be smaller compared to using the bias-adjusted LST which is also not suitable for the downscaling theory we base as the theory was actually developed for clear-sky condition.
Line 326: One or two sentences for briefly summarizing the downscaling methodology in Song et al. 2021 are necessary.	Accepted and added. Please see Lines 334-338
Line 329: SEE, "soil evaporative efficiency"	Done as suggested.
Line 346: "All pixels were utilized within ... centered at ..." would be better	Done as suggested.
Line 369: can you explain what "spatial averaging disaggregation" is	Sorry for this mistake. We have revised it as "spatial averaging operator for..."
Line 417: why the bias caused by heterogeneity is negative?	We actually mean the effect is "not beneficial", but not mean it has a "negative-sign bias". Now we have

	revised it to “disadvantageous effects” (Line 438)
Line 431: why RMSD_diff is important and focused? Maybe both clear-sky and cloudy-sky LSTs have higher uncertainty at some locations but the difference is small.	The main technical issues to tackle for generating this SSM product include gap-filling of LST under cloud, but not include retrieval of LST under clear sky. In other words, our work relies on the general accuracy of the existing LST product under clear sky (MODIS 1-km LST), which has been generally evaluated by Fig.3-(a) for the overall situation. As the primary purpose is to obtain LST of complete-coverage with consistent accuracy for all-weather conditions, the RMSD_diff is most important compared to other metrics. Based on the above concern, we made an extra site-based analysis for RMSD_diff in Fig.3-(c), while for the absolute RMSD values, the all-site analyses in Fig.3-(a) and –(b) are sufficient.
Fig 3: the absolute accuracy numbers of Fig 3(a) and (b) are better to be listed in the figure	Done as suggested.
Line 436: I feel 1.9 K is not small, and the RMSD difference can be ~70% of the clear-sky LST absolute accuracy [<i>Xu and Cheng, 2021; Zhang et al., 2021</i>], especially for the nighttime LST. The word ‘only’ is too strong.	Accepted. We removed the word “only”. We also changed the following sentence from “small uncertainty” to “uncertainty is not very significant”. (Lines 458-460)
Fig 5, Line 663: please unify the ubRMSD or ubRMSE in the context.	Done as suggested.

Reference

- Das, N. N., Entekhabi, D., Dunbar, R. S., Chaubell, M. J., Colliander, A., Yueh, S., . . . Thibeault, M.: The SMAP and Copernicus Sentinel 1A/B microwave active-passive high resolution surface soil moisture product, *Remote Sens. Environ.*, 233, 111380, <https://doi.org/10.1016/j.rse.2019.111380>, 2019.
- Mohammad, E. H., Nicolas, B., Mehrez, Z., Nemesio, R. F., Jean, W., Amen, A. Y., . . . Jean-Christophe, C.: Evaluation of SMOS, SMAP, ASCAT and Sentinel-1 Soil Moisture Products at Sites in Southwestern France, *Remote Sens.*, 10, 569, 2018.

Author Response to RC2

Journal: ESSD

Title: A 1-km daily surface soil moisture dataset of enhanced coverage under all-weather conditions over China in 2003-2019

Author(s): Peilin Song et al.

MS No.: essd-2021-428

MS Type: Data description paper

General Comments:

“The authors present a downscaled soil moisture product, which combines the advantages of a 36-km resolution passive microwave remote sensing product with a 1-km resolution MODIS LST product. Such high-resolution soil moisture is very important for agriculture and water resource management. The manuscript is generally well-organized, I suggest accepting it with considering the following revisions.”

Response:

All authors greatly appreciate you for your final decision with “accepting it with considering the following revisions”. We have paid great attentions on each bullet pointed out by you and have modified our paper carefully based on your comments. Please see the following responses to your specific comments.

Response to specific comments

1. The quality of the figures should be improved. Currently, some legends are too small to identify.

Response:

We have tried to improve the quality of some figures (Fig.3, Fig.5, Fig. 7). However, if there are still unclear legends in the figures, please let us know the specific points after this revision. Thank you.

2. Fig. 7. was not used in the main text.

Response:

We accept your comment and have mentioned Fig.7 as “another manner of illustrating Fig.6” in the revised version, above Fig.6 and Fig.7. Please see Lines 544-547 (*“The above inter-seasonal differences on data coverage are also reflected in Fig. 7 in another manner based on presenting the spatial distributions of number percentages of available dates in each three-month period”*).

3. Also in Fig.7., it shows that the original PM SSM almost does not have any data in the winter season on the Tibetan Plateau. It is reasonable since, in the winter season, the soil is frozen and generally covered by snow, and then it is difficult for microwave remote sensing to identify soil moisture. However, as shown in this figure, the new 1-km downscaling product has some soil moisture data. How did it come? What did the soil moisture value during this season on the Tibetan Plateau mean? How about the accuracy of these downscaled SSM?

Response:

Thank you for reminding us on this problem. Our downscaling framework is actually consistent with your opinion on leaving out the invalid “winter pixels” (See our description in Lines 538-542). Unfortunately, we made a tiny technical mistake when calculating the statistics for Fig. 6 and Fig.7 last time. Now the bug has been fixed for both Fig. 6 and Fig. 7. Also, relevant texts have been revised (please see Line 535). In this revised version, null values have been assigned for all 1-km sub-pixels within the frozen or snow-covered passive microwave pixels (e.g. the microwave pixels characterized by null values on the Tibetan Plateau in winter and early spring).

4. It is recommended to draw some time series of the soil moisture products, the new one, the original one, and SMAP high resolution one, on several stations, to demonstrate the advantages of this daily 1-km product.

Response:

Thanks for your advice. We had actually investigated the time series at some of the stations when we designed this study. After careful investigation, however, we found it is rather difficult to use time series data at only a few stations to highlight our conclusions that have been drawn based on nation-wide research. We do not wish to have an impression of cherry picking. Therefore, we finally decided not to present any of them in the paper:

(1) In our study we have more than 2000 validation sites across the country in total. The time series patterns for the downscaled SSM and the station benchmarks are rather different from site to site. It's very difficult to find one or two sites where the relative performances

among soil moisture time series of different data sources are typical and representative of their background climate regions at the provincial or large-basin levels. Moreover, we believe the complicated influential factors behind soil moisture seasonal time series of different eco-regions have to be investigated specifically in our subsequent studies. For our current study case, the overall validation performance (see Fig.4) is more important than time series demonstration.

(2) The SMAP-sentinel high resolution data has a much poorer temporal frequency (for some locations even lower than 12 days), as a consequence of which, the true shape of its time series might be arbitrarily interpreted. Therefore, it is difficult to fairly compare its time series with that of other daily-scale datasets through visual inspection.

A 1-km daily surface soil moisture dataset of enhanced coverage under all-weather conditions over China in 2003-2019

Peilin Song^{1,4}, Yongqiang Zhang^{1*}, Jianping Guo^{2*}, Jiancheng Shi³, Tianjie Zhao⁴, Bing Tong²

¹ Key Laboratory of Water Cycle and Related Land Surface Processes, Institute of Geographic Sciences and Natural Resources Research, The Chinese Academy of Sciences, Beijing 100101, China

² State Key Laboratory of Severe Weather, Chinese Academy of Meteorological Sciences, Beijing 100081, China

³ National Space Science Center, Chinese Academy of Sciences, Beijing 100190, China

⁴ State Key Laboratory of Remote Sensing Science, Aerospace Information Research Institute, Chinese Academy of Sciences, Beijing 100101, China

**Correspondence to:* Yongqiang Zhang (yongqiang.zhang2014@gmail.com);
Jianping Guo (jpguo@cma.gov.cn)

21

22 **Abstract:**

23 Surface soil moisture (SSM) is crucial for understanding the hydrological process of
24 our earth surface. Passive microwave (PM) technique has long been the primary tool
25 for estimating global SSM from the view of satellite, while the coarse resolution
26 (usually >10 km) of PM observations hampers its applications at finer scales.
27 Although quantitative studies have been proposed for downscaling satellite PM-based
28 SSM, very few products have been available to public that meet the qualification of 1-
29 km resolution and daily revisit cycles under all-weather conditions. In this study, we
30 developed one such SSM product in China with all these characteristics. The product
31 was generated through downscaling the AMSR-E/AMSR-2 based SSM at 36-km,
32 covering all on-orbit time of the two radiometers during 2003-2019. MODIS optical
33 reflectance data and daily thermal infrared land surface temperature (LST) that had
34 been gap-filled for cloudy conditions were the primary data inputs of the downscaling
35 model, so that the “all-weather” quality was achieved for the 1-km SSM. Daily images
36 from this developed SSM product have quasi-complete coverage over the country
37 during April-September. For other months, the national coverage percentage of the
38 developed product is also greatly improved against the original daily PM observations,
39 through a specifically developed sub-model for filling the gap between seams of
40 neighboring PM swaths during the downscaling procedure. The product is well
41 compared against *in situ* soil moisture measurements from 2000+ meteorological
42 stations, indicated by station averages of the unbiased RMSD ranging from 0.052

vol/vol to 0.059 vol/vol. Moreover, the evaluation results also show that the developed product outperforms the SMAP-Sentinel (Active-Passive microwave) combined SSM product at 1-km, with a correlation coefficient of 0.55 achieved against that of 0.40 for the latter product. This indicates the new product has great potential to be used for hydrological community, agricultural industry, water resource and environment management.

1. Introduction

Surface soil moisture (SSM) is one of the most important variables that dominate the mass and energy cycles of earth surface system (Entekhabi et al., 2010b). Satellite-based SSM datasets of sufficiently fine spatio-temporal resolutions over large-scale areas have significant implication on improved investigations at various research fields including hydrological signature identification (Zhou et al., 2021; Jung et al., 2010), agricultural yield production estimation (Ines et al., 2013; Pan et al., 2019), drought/waterlogging monitoring and warning (Vergopolan et al., 2021; Den Besten et al., 2021; Jing and Zhang, 2010), as well as weather prediction and future climate analysis (Koster et al., 2010; Jeffrey et al., 2001). Microwave bands with centimeter-level or longer wavelengths (X-band, C-band, and L-band) are currently identified as the primary band channels suitable for SSM observations from view of satellite, due to their high penetration capabilities through cloud layers and vegetation canopies. In terms of sensor types, microwave SSM detection includes passive microwave (radiometer-based) techniques and active microwave (radar, scatterometer) techniques.

Satellite-based passive microwave (PM) radiometers, e.g. the Soil Moisture Active Passive (SMAP), the Soil Moisture and Ocean Salinity (SMOS), and the Advance Microwave Scanning Radiometer-2 (AMSR-2), can obtain SSM observations at a revisit interval of 1-3 days, with relatively poor native spatial resolutions of tens of kilometers. Active microwave (AM) such as radar can achieve kilometer-level and even finer resolution of observations targeting at the earth surface. However, this usually sacrifices the swath width of radar configuration, because of which, most satellite-based synthetic aperture radars (SAR) have an obviously longer global revisit cycle (usually longer than 5 days, e.g. Sentinel-1 SAR data) than the typical radiometers. Moreover, AM radar backscatter signals are extremely sensitive to speckle noise (Entekhabi et al., 2016), as well as influence from soil roughness, vegetation canopy structure and water content (Piles et al., 2009). All above influential factors have seriously impeded the use of AM radar techniques or combination of passive/active microwave datasets for producing high spatial resolution SSM products with a frequent revisit.

Apart from microwave signals, solar reflectance or ground emission signals originated from optical and infrared band domains also have the potential to reflect SSM variation. Based on optical/infrared bands, however, SSM is typically estimated based on indirect relationships through intermediate variables like soil evaporation (Komatsu, 2003), vegetation condition (Zeng et al., 2004), or soil thermal inertia (Verstraeten et al., 2006). To overcome the spatio-temporally instable performance on SSM modelling that might be brought by such indirect relationships, they are typically fused with the PM SSM datasets. In this manner, it can well reconcile the advantage of

PM observations with respect to its high sensitivity to SSM variation, as well as that of optical/infrared observations with respect to its finer spatial resolutions at kilometer- or even hectometer-levels. Such data fusion techniques are also known as downscaling techniques of PM remote sensing SSM. Archetypal downscaling models include the “[universal](#) triangle feature space (UTFS)”-based models (Chauhan et al., 2003; Choi and Hur, 2012; Sanchez-Ruiz et al., 2014), the “DISaggregation based on a Physical And Theoretical scale CHange (DISPACTH)” model (Merlin et al., 2010; Merlin et al., 2005; Merlin et al., 2013; Merlin et al., 2008), and the “[University of California, Los Angeles \(UCLA\)](#)” model (Peng et al., 2016). The physics of these models are mainly based on the response of SSM variation to changes in soil evaporation or land surface evapotranspiration. Another significant branch of such downscaling models are based on the sensitivity of SSM to soil thermal inertia, which is quantified by diurnal LST difference estimated from thermal-infrared wave bands (Fang and Lakshmi, 2013; Fang et al., 2018).

Sabaghy et al. (2020) have shown that using optical and infrared data can achieve finer-resolution SSM estimates which are better consistent with ground soil moisture records, compared with using the radar datasets. Moreover, considering the short revisit cycle (daily) of optical/infrared sensors onboard typical polar-orbit satellites, using optical/infrared datasets to downscale PM SSM should be among the optimal methods for obtaining SSM data with high spatio-temporal resolutions over national, continental, or global scales. On the other hand, satellite remote sensing SSM products that are characterized by 1-km resolution of daily revisit intervals and stable long time series

108 dating back to at least 15-20 years ago, are urgently required for accelerating the
109 development of various research fields, especially agriculture industry, water resources
110 management, and hydrological disaster monitoring (Sabaghy et al., 2020; Mendoza et
111 al., 2016). However, very seldom sets of such data products are publicly available to
112 the remote sensing research community because of the following drawbacks. First,
113 there is a serious lack of cloud-free optical/infrared imagery, which means the method
114 cannot deliver any SSM downscaling under cloudy/rainy weather. Second, most of the
115 above-mentioned optical/infrared-data-based downscaling methods were mainly
116 evaluated at regional or even smaller scales. This might raise concern on the
117 universality of those methods. For example, the DISPATCH method has been
118 recognized to be less effective in humid (energy-limited) regions compared with in arid
119 and semi-arid (water-limited) regions (Molero et al., 2016; Song et al., 2021; Zheng et
120 al., 2021). As far as the UTFS-based method is concerned, a poorer performance was
121 obtained compared to the DISPATCH in a typical water-limited region in North
122 America, according to the experiment conducted by Kim and Hogue (2012).

123 To improve the above-mentioned issues, we produced an all-weather daily SSM
124 data product at 1-km resolution all over China during 2003-2019, based on fusion of
125 multiple remote sensing techniques, including reconstruction of optical/infrared
126 observations under cloud as well as an improved PM SSM downscaling methodology
127 proposed in our previous study (Song et al., 2021). The potential significance of this
128 study includes

(i) to better serve and investigate the land surface hydrology processes and their sophisticated interactions to human society at multi-scale (from national to regional) resolutions in China because the country covers about 1/15 of the global terrestrial area with about 1/5 of the world population, and

(ii) to provide a methodology framework that can inspire future studies on generating similar SSM datasets all over the globe, based on the plentifulness of resources on climate type, land covers, and topography in China.

2. Methods and Materials

2.1 Datasets

2.1.1 PM SSM data

Spatial downscaling of PM SSM is the fundamental theory for constructing the target finer-resolution data product in this study. Therefore, the native retrieval accuracy of the coarse-resolution PM SSM data product, based on which the downscaling procedures are performed, is considerably crucial to the performance of the downscaled data product (Busch et al., 2012; Im et al., 2016; Kim and Hogue, 2012). Although the L-band PM brightness temperature (TB) observed by satellite missions such as SMAP or SMOS are considered more suitable for SSM retrieval compared with C- or X-band TB, both above missions started their space operations [after-in the](#) 2010s. This means that to obtain downscaled SSM of longer historical periods, we still require to rely on other C-/X-band-based radiometers which started their operations earlier than

SMAP and SMOS. An optimal satellite PM TB observation system dating back to earlier years of this century is composed of the “Advanced Microwave Scanning Radiometer of the Earth Observing System (AMSR-E)”, together with its successor of AMSR-2. AMSR-E operated during 2002-2011 onboard the Aqua satellite which is governed by National Aeronautics and Space Administration (NASA), whilst AMSR-2 is operating onboard the Global Change Observation Mission1-Water (GCOM-W1) satellite developed by the Japan Aerospace Exploration Agency (JAXA) since 2012.

Several classical PM SSM retrieval algorithms have been applied to the aforementioned “AMSR series (including AMSR-E and AMSR-2)” TB for generating long-term global SSM products at 25 km ([Table 1](#)~~Table 1~~), including the JAXA algorithm (Fujii et al., 2009; Koike et al., 2004), the “Land Parameter Retrieval Model (LPRM)” algorithm (Song et al., 2019b; Meesters et al., 2005; Owe et al., 2001), and the algorithm developed by the University of Montana (UMT) (Jones et al., 2009; Du et al., 2016). A recent AMSR-based night-time SSM product during 2002-2019 has been produced through a neural network trained against SMAP descending SSM (hereafter referred to as “NN-SM product”) (Yao et al., 2021). The global validation results show that this NN-SM product is better than the JAXA and LPRM products.

Besides, the NN-SM has also been compared with another long-term ~25-km all-weather SSM dataset generated through the European Space Agency (ESA)’s Climate Change Initiative (CCI) program. The ESA-CCI SSM product is different from the rest products mentioned above in that it was implemented by fusion of observations from comprehensive AM- and PM-based satellite sensors, rather than only relying on the

radiometers of AMSR series. According to Yao et al. (2021), the ESA-CCI SSM has slightly better validation accuracy than the NN-SM product, but the number of available observations per pixel cell in an entire year is much smaller for the ESA-CCI SSM in Southeast China. In view of all above coarse-resolution SSM data products, we finally selected the NN-SM product to implement the following spatial downscaling procedures rather than the ESA-CCI SSM, to make a balance between data accuracy and data availability per year. We have also made additional evaluations within China in Section Appendix-A to ensure the relatively outstanding performance of the NN-SM product as described above.

Table 1 Information of all-weather microwave remote sensing coarse-resolution SSM data products that can be potentially downscaled to obtain high-fine resolution SSM.

Name	Resolution	Satellite radiometers involved	Data availability (URL)
NN-SM product	36 km (by the EASE Grid projection)	AMSR-E/ AMSR-2 (2002-2011, 2012-present)	https://data.tpsc.ac.cn/en/data/c26201fc-526c-465d-bae7-5f02fa49d738/
ESA-CCI v6.1 product	0.25°	AMSR-E/ AMSR-2/ SMOS/ WindSat/ SMMR/ SSM/I/ TMI (1978-2020)	https://www.esa-soilmoisture-cci.org/v06.1_release
JAXA product	0.25° / 0.1°	AMSR-E/ AMSR-2 (2002-2011, 2012-present)	https://gportal.jaxa.jp/
LPRM product	0.25° / 0.1°	AMSR-E/ AMSR-2 (2002-2011, 2012-present)	https://search.earthdata.nasa.gov/
UMT product	25 km (by the EASE Grid projection)	AMSR-E/ AMSR-2 (2002-present)	http://files.ntsg.umd.edu/data/LPDR_v2/

2.1.2 Optical remote sensing data and digital elevation model (DEM)

Optical remote sensing datasets provide finer spatial texture information on the daily basis for the downscaling purpose of PM SSM. Such data that can be used as inputs of our SSM product processing line are mainly provided by the Moderate-resolution Imaging Spectroradiometer (MODIS) onboard the Terra and Aqua satellites. Specifically, they involve the 1-km daily night-time Aqua MODIS LST product (MYD21A1N.v061) and the 500-m daily “Bidirectional Reflectance Distribution Function (BRDF)” - Adjusted Reflectance dataset (MCD43A4.v061). MYD21A1 LST data can be recognized as a crucial proxy of land surface thermal capacity (Fang et al., 2013) and soil evaporative rate (Merlin et al., 2008). The MCD43A4 nadir reflectance product, with view angle effect corrected using the BRDF model, is capable to provide observations from visible to shortwave-infrared bands that can characterize water content variation of the bare soils as well as the vegetation canopy. Overall, the above-mentioned datasets were selected primarily because they deliver indicators (land surface thermal capacity, soil evaporative rate, or vegetation condition) that can well response to soil moisture dynamics from different aspects. Prior to being employed for SSM downscaling, conventional pre-processing procedure of pixel quality check was applied for both optical products by screening out pixels not classed as “good quality”, according to the 8-bit “Quality Assessment (QA)” field of each spectral band. Moreover, to normalize their natively different spatial resolutions, all MCD43A4 based reflectance

values at the 500-m pixel level were upscaled to the sinusoidally projected MODIS 1-km grids using their spatial averages.

Apart from MODIS optical remote sensing data, all 90-m DEM tiles generated by the NASA Shuttle Radar Topography Mission (SRTM; <http://srtm.csi.cgiar.org/>, last access: July 10, 2020) were mosaicked ~~over the entire~~ all over China and then employed as another essential input variable for the procedures as described by Section 2.2.2 below. Similar to that applied to the MCD43A4 product, spatial upscaling in correspondence to the MODIS 1-km grids is also an indispensable pre-processing step for the mosaicked DEM data.

2.1.3 Ground validation data

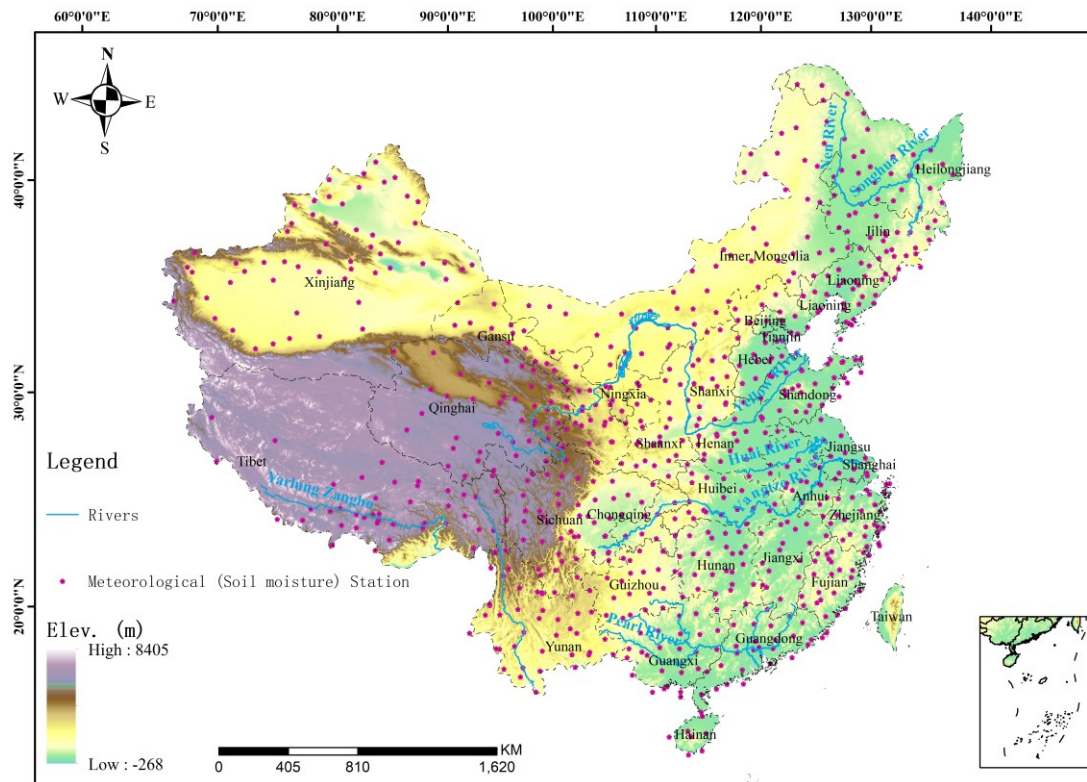


Fig. 1 The provincial-level administration map of China superposed with topographic information, as well as general locations for the 756 basic meteorological stations (<http://data.cma.cn/>, last access: January 20, 2021) that provide partial benchmark measurements for SSM and LST validation in this study.

We utilized ground soil moisture measurements for validating the downscaled remote sensing SSM product. The ground measurements are derived from 756 meteorological stations (including 756 basic stations of the National Climate Observatory and 1661 regionally intensified stations) of over China, as partially shown in Fig. 1. The soil moisture measurement devices in these stations, with uniform observation standards, are instrumented under the national project of “Operation Monitoring System of Automatic Soil Moisture Observation Network in China (Wu et al., 2014)”, the construction of which has been led by China Meteorological Administration since 2005. Until 2016, all stations have been in operation for

229 automatically observing hourly in situ soil moisture dynamics at eight different depth
230 ranges (0-10 cm, 10-20 cm, 20-30 cm, 30-40 cm, 40-50 cm, 50-60 cm, 70-80 cm, 90-
231 100 cm). It has also been widely used by previous studies for evaluating satellite soil
232 moisture estimates in China (Meng et al., 2021; Chen et al., 2020; Zhang et al., 2014;
233 Zhu and Shi, 2014). ~~for evaluation of satellite soil moisture estimates in China.~~ In our
234 current study, ground measurements matching the shallowest depth range (0-10 cm)
235 from the initial time of each station until the end of 2019 are employed as validation
236 benchmark of the satellite SSM retrievals. At the temporal dimension, measurements
237 made at 1:00 A.M. and 2:00 A.M are averaged, in order to match the mean satellite
238 transit time of 1:30 A.M. for AMSR descending observations.

239 Moreover, 0-cm top ground temperatures are simultaneously measured at all these
240 meteorological stations on the daily basis, at the local time windows of 2:00 A.M./P.M.
241 and 10:00 A.M./P.M., respectively. We therefore exploited such measurements
242 recorded at 2:00 A.M. to validate the cloud gap-filled night-time (~1:30 A.M.) LST
243 estimates over the Aqua-MODIS based 1-km pixels containing these stations (see
244 Section 2.2.2). Our primary validation period covers the entire years of 2017, 2018, and
245 2019.

246 2.1.4 Ancillary SSM products for comparison

247 In order to comprehensively demonstrate the validation performance of our
248 proposed SSM product, there is necessity to make an inter-comparison against similar
249 existing datasets. In this regard, we introduced the Level2 SMAP/Sentinel Active-

Passive combined SSM product on 1-km earth-fixed grids, i.e., the SPL2SMAP_S_V3 dataset (Das et al., 2020), and used its validation performance against in-situ measurements throughout the years of 2017, 2018, and 2019, as a baseline to better evaluate our proposed SSM product. The SPL2SMAP_S_V3 dataset contains global SSM at resolutions of 3 km and 1 km respectively, which were disaggregated from the SMAP SSM retrievals of 36-km/9-km footprints in conjunction with the high-resolution Sentinel-1 C-band radar backscatter coefficients (Das et al., 2019). To our knowledge, this dataset is possibly the only publicly available product which can provide global remote sensing SSM estimates at the 1-km resolution. The sentinel backscatter coefficient inputs for this product are only those received in the descending orbit scenes (at ~6:00 A.M. of local time), whilst the closest SMAP SSM retrievals from either ascending (at ~6:00 P.M. of local time) or descending orbits are used to spatially match up with the sentinel-1 scene. It is noticed that at the descending observation time the soil moisture vertical profile has approached a hydrostatic balance (Montaldo et al., 2001), thereby providing the optimal chance for soil moisture fusion and validation with observations at different soil depths. Therefore, we only selected the 1-km disaggregated SSM estimates based on descending SMAP SSM retrievals (i.e., the subset with field name of ‘disagg_soil_moisture_1 km’ in the SPL2SMAP_S_V3 dataset). Meanwhile, the ~~10-cm-depth~~0-10 cm in-situ soil moisture measurements observed at 6:00 A.M. were employed as the validation benchmark, in a manner similar to that applied to our proposed SSM product (Section 2.1.3).

2.2 Methodology

The general methodological framework for producing the all-weather daily 1-km SSM product is shown as in Fig. 2, with details described in the following context of this section.

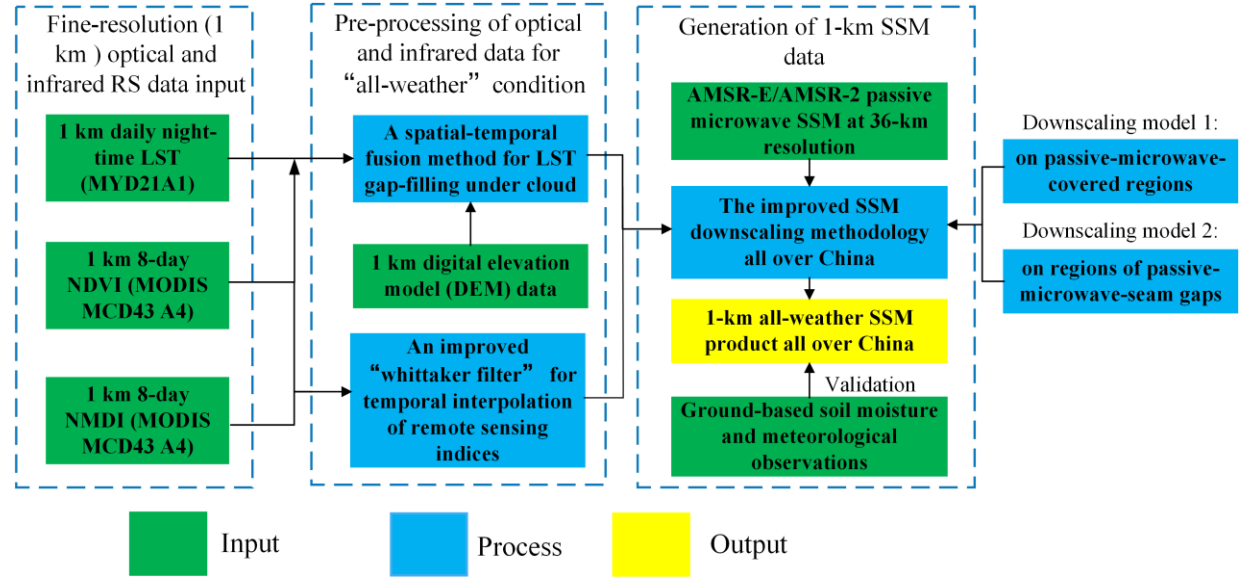


Fig. 2 The overall methodological framework of this study.

2.2.1 Reconstruction of thermal-infrared LST and remote sensing (vegetation) indices under cloud

Reconstruction of missing pixels under cloud in the optical remote sensing input datasets is the prerequisite for achieving the “all-weather” property of the final downscaled SSM output. For reconstructing thermal-infrared LST, we adopted the cloud gap-filling method as proposed by our previous study (Song et al., 2019a). This method, also referred to as a typical “spatio-temporal data fusion” (STDF) method (Dowling et al., 2021), was built using clear-sky LST observations of spatially neighboring pixels observed at proximal dates, with concurrent NDVI and DEM also employed as additional data inputs. The STDF method can be expressed as follows:

$$LST_{t_1}^* = a \times LST_{t_0}^* + b \times NDVI_{t_1}^* + c \times DEM^* + d \quad (1)$$

Where the superscript “*” indicates that this variable has been normalized to the range 0 to 1.0 (Song et al., 2019a), based on the maximum and minimum values of that variable found across China (excluding invalid values representing states of snow, ice, and water bodies). Parameters a , b , c , and d are coefficients fitted between all pixels with clear-sky LST estimates on a specific date t_l ($LST^*_{t_l}$) and their counterparts on one proximal date, t_0 ($LST^*_{t_0}$). $NDVI^*_{t_l}$ indicates the corresponding (normalized) NDVI on the t_l date calculated using the MCD43A4 daily product. After deriving the coefficients of a , b , c , and d , Equation (1) was used to fill all cloudy MODIS LST pixels on the t_l date. For any t_l date included in the study period, the t_0 date was iterated among all neighboring dates of t_l meeting the condition $|t_0 - t_l| \leq 30$ (from the nearest date to the furthest date). The average of estimated LST values for t_0 was then taken where a cloud gap pixel was filled more than once (based on the iterative t_0 dates). The iteration was stopped when the fraction of pixels with effective LST values on t_l was equal to or exceeded 0.99.

An important flaw of this STDF method should be noticed with regard to potentially existential bias of the cloud gap-filled LST outputs, because the outputs represent theoretically reconstructed LST under clear sky rather than under the real cloudy condition. Another of our previous studies (Dowling et al., 2021) concerning this STDF method proposed a follow-up step, which incorporated PM-derived surface temperature, to adjust that bias. In our current production pipeline, however, this follow-up step for cloud bias adjustment in LST was not carried out. This is because the results in Section Appendix-B show that using LST generated by the STDF alone leads to more accurate SSM outcomes in general. –The possible reasons for this are discussed below in Section 4.2. This is mainly because the gap-filled LST outputs are intended for SSM downscaling. The downscaling techniques as proposed in Section

~~2.2.1 was developed based on the “universal triangle feature (UTF)” theory (Carlson et al., 1994). In the UTF, clear-sky LST was employed to quantify the land surface evaporation when vegetation cover density was fixed. The degree of land surface wetness was then predicted implicitly through soil evaporation degree and surface soil thermal inertia. Under cloudy conditions, however, the satellite-observed LST would be a proxy of not only surface soil property, but also of that related to cloud liquid water and crystals in the atmospheric layers. In comparison, therefore, LST generated by the STDF alone for clear-sky conditions would be a more competent input variable for quantifying surface soil wetness under cloudy conditions. We have made additional evaluations to confirm the validity of this assumption, with the results elaborated in Section Appendix B of this paper.~~

Reconstruction of the remote sensing vegetation indices under cloudy conditions, including NDVI and MNDI, was simply based on the modified time series filter of the Whittaker Smoother (MWS) as developed by Kong et al. (2019). This is reasonable because the dynamic trends of vegetation growth are relatively less volatile compared to LST on the daily basis, and can thus be gap-filled for missing values using a time-series-filtering-like algorithm.

2.2.2 Improved downscaling technique of SSM based on fusion of PM and optical/infrared data

The core component of the SSM downscaling methodology is an improved linking model between PM SSM and (fine-resolution) optical remote sensing observations. This model enhances the relatively poorer performance of the conventional DISPATCH in energy-limited regions, whilst maintains the generally good quality of the DISPATCH in water-limited ones. Therefore, the improved model is more appropriate

to be applied in China which contains a wide range of geographical settings, compared to other conventional downscaling models. Since this model originates from our previous

study (Song et al., 2021), herein we simply give its mathematical expression as follows:

$$SSM = \frac{a \times \ln(1 - SEE)}{1 - b \times NMDI} + c \quad (2)$$

In Equation (2), *SEE* denotes “soil evaporative efficiency” and is a mathematical function of LST and the typical Normalized Difference Vegetation Index (NDVI), with its specific form described in Merlin et al. (2008). NMDI is another remote sensing index calculated as $\frac{R_{infr,860nm} - (R_{sw,1600nm} - R_{sw,2100nm})}{R_{infr,860nm} + (R_{sw,1600nm} - R_{sw,2100nm})}$ (Wang and Qu, 2007).

$R_{infr,860nm}$, $R_{infr,1600nm}$, and $R_{infr,2100nm}$ represent land surface reflectance signals derived from three different MODIS-MCD43A4 based near-infrared/shortwave-infrared bands, with their wavelengths centering at 860 nm, 1600 nm, and 2100 nm respectively. The parameters a , b , and c are empirical coefficients that represent background information of local soil texture and vegetation types. In Song et al. (2021), these coefficients have been fitted and calibrated based on multi-temporal observations at the PM pixel scale. In our current study, however, we have discovered that coupling of multiphase observations at both the spatial and the temporal dimensions can lead to more optimal solution of the coefficients, as they can produce downscaled SSM images with notably declined effect of ‘mosaic’ against the original PM 36-km pixels. Therefore, the modified optimal cost function χ^2 for deriving these coefficients is re-defined as follows:

$$\chi^2 = \sum_{d=-dl}^{dl} \sum_{i=0}^{N=ws \times ws} w_i \times (SSM_{ob,i,d} - SSM_{mod,i,d})^2$$

(3)

Through the cost function, the spatial extent of each 36-km pixel P_0 on any arbitrary date D_0 obtains a unique set of coefficients. As shown by Equation (3), all pixels were exploited within the $N=7 \times 7$ spatial square window (with its side length equal to ws) centered at P_0 ranging from $-5th-dl-th$ day to $dl-5th$ day relative to the date of D_0 were exploited. To determine the optimum values for dl and ws , we have tested each member in the collection of [3, 5, 7, 9, 11, 13] for both of the parameters. Through evaluation against in-situ data indicates that the optimum dl and ws are 5 and 7, respectively (which is like that results are similar to what is shown in Section 3.2, but is not demonstrated not presented here in this paper). the optimum dl and ws are set as 5 and 7 respectively. SSM_{ob} and SSM_{mod} denote the AMSR NN-SM 36-km SSM observations as well as SSM observations modelled by Equation (2) based on upscaled optical datasets, respectively. w_i is a weight coefficient used to ensure that neighboring observations near the centering pixel P_0 play more dominating roles as compared with the far-end pixels in the cost function, considering the ‘‘Tobler’s First Law of Geography (Sui, 2004)’’. w_i is calculated using an adaptive bi-square function:

$$w_i = [1 - (\frac{dis_i}{b})^2]^2, dis_i < b$$

$$w_i = 0, dis_i \geq b$$

(4)

where dis_i indicates the distance between the $i-th$ pixel and the centering pixel P_0 . b is named as the adaptive kernel bandwidth of the bi-square function (Duan and Li, 2016),

and is optimized as 200 km through using a cross validation method as recommended by Brunsdon et al. (1996).

With the linking model obtained, we can subsequently utilize the spatial downscaling relationship function to produce 1-km [high-fine](#) resolution SSM. The downscaling relationship function is constructed by transforming the linking model into its Taylor expansion formula and preserving all components with respect to the input optical variables of the linking model at first and second orders. This relationship is inspired from Malbêteau et al. (2016) and Merlin et al. (2010), and is mathematically described below:

$$SSM_{1km} = SSM_{36km} + \left(\frac{\partial SSM}{\partial SSE} \right)_{36km} \times (SSE_{1km} - \langle SSE \rangle_{36km}) + 0.5 \times \left(\frac{\partial^2 SSM}{\partial SSE^2} \right) \times (SSE_{1km} - \langle SSE \rangle_{36km})^2 + \left(\frac{\partial SSM}{\partial NMDI} \right)_{36km} \times (NMDI_{1km} - \langle NMDI \rangle_{36km}) + 0.5 \times \left(\frac{\partial^2 SSM}{\partial NMDI^2} \right) \times (NMDI_{1km} - \langle NMDI \rangle_{36km})^2 \quad (5)$$

In the above relationship, $\langle \rangle$ denotes the [spatial averaging](#) operator ~~of spatial averaging~~ [disaggregation](#) for [all of](#) the 1-km optical remote sensing input variables ~~at within~~ the corresponding 36-km pixel, $\frac{\partial SSM}{\partial SSE}$ $\left(\frac{\partial^2 SSM}{\partial SSE^2} \right)$ and $\frac{\partial SSM}{\partial NMDI}$ $\left(\frac{\partial^2 SSM}{\partial NMDI^2} \right)$ respectively denoting the first-(second-) order partial derivative of the linking model described in Equation (2).

It should be noticed that there exist middle-/low-latitude gap regions between seams of neighboring daily AMSR-E(-2) swaths, indicating that SSM_{36km} in Equation (5) is not always available on the daily basis (Song and Zhang, 2021b). For such PM-seam gaps on a particular date t_0 , the corresponding SSM_{36km,t_0} in Equation (5) is substituted by $0.5 \times (SSM_{36km,t_0+1} + SSM_{36km,t_0-1}) + \Delta SSM_{36km,t_0}$. Herein SSM_{36km,t_0-1}

and $SSM_{36km,t0+1}$ respectively denote the SSM estimate before and after the date of t_0 .

$\Delta SSM_{36km,t0}$ is a component for correcting inter-day bias, with the following expression:

$$\Delta SSM_{36km,t0} = SSM(SEE_{36km,t0}, NMDI_{36km,t0}) - 0.5 \times (SSM(SEE_{36km,t0-1}, NMDI_{36km,t0-1}) + SSM(SEE_{36km,t0+1}, NMDI_{36km,t0+1})) \quad (6)$$

In the above equation, $SSM(SEE_{36km}, NMDI_{36km})$ denotes SSM that is directly modelled based on Equation (1) using 36-km SEE and NMDI. The 36-km SEE and NMDI are obtained via averaging the variables spatially from their native resolution at 1-km. If all SSM_{36-km} during the three consecutive days (t_0-1 , t_0 , and t_0+1) are missing due to other extreme conditions like snow, ice, or surface dominated by substantially large water bodies, the downscaling process cannot be fulfilled and all 1-km sub-pixels with the SSM_{36-km} have to be set as null values.

2.2.3 Evaluation metrics

We employed the classic metrics of ‘Root Mean Square Difference (RMSD)’ and correlation coefficient (r -value) for evaluating satellite-based (SSM and LST) estimates against ground measurements. Herein RMSD is not referred to as ‘Root Mean Square Error (RMSE)’, although the latter term shares the same definition and has been used more commonly in previous studies. This is because the ground benchmark data may also present measurement uncertainties in practice. For SSM evaluation, the unbiased RMSD, or ubRMSD (Entekhabi et al., 2010a; Molero et al., 2016), is calculated instead of RMSD in order to better investigate the time series similarity between satellite and ground soil moisture datasets by eliminating the systematic bias caused by spatial scale mismatch between them.

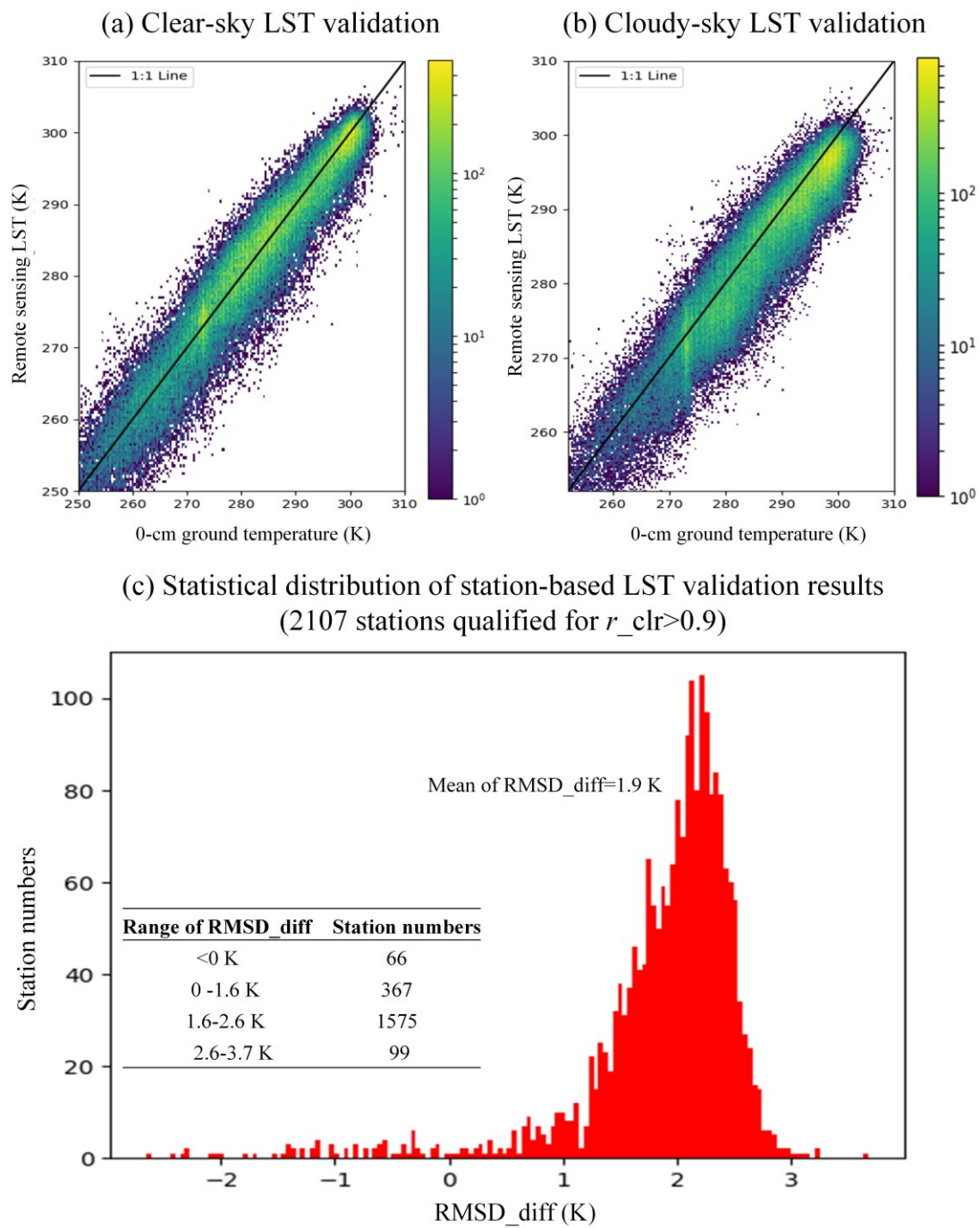
The above-mentioned classic metrics are primarily suitable to evaluate the absolute reliability of an independent remote sensing product. However, we also require another metric for characterizing the relative improvement of the downscaled SSM estimates against the original PM observations on capturing local soil moisture dynamics. For this purpose, we employed the “gain metric” of G_{down} , which was developed particularly by Merlin et al. (2015) for assessment of soil moisture downscaling methodology. G_{down} is a comprehensive indicator for evaluating gains of the downscaled SSM against the original coarse-resolution PM data in terms of their mean bias, bias in variance (slope), and time series correlation with ground benchmark. It has a valid domain between -1 and 1, with positive (negative) value indicating improved (deteriorated) spatial representativeness of the downscaled SSM against the original PM data. Detailed definition and introduction of G_{down} are given in Equation (8) and Section 3.3 of Merlin et al. (2015).

3. Results

3.1 Evaluation on reconstructed thermal-infrared LST under cloud

The meteorological-station-based validation of reconstructed 1-km thermal-infrared LST under cloud were preliminarily fulfilled, to ensure the high quality of input dataset variables for SSM downscaling. Since ~~disadvantageous~~ ~~negative~~ effects might be brought to this validation campaign by the potentially existing heterogeneity of the validated 1-km thermal-infrared remote sensing pixels, we firstly analyzed correlations

between estimated and benchmark datasets at each station, only based on satellite remote sensing observations obtained under clear sky. Stations that have their correlation coefficients (r_{clr}) lower than 0.9 herein have to be screened out because there exist higher chances of cross-scale spatial mismatch within and around these stations in terms of the land surface thermal properties. Among all 2417 stations (see Section 2.1.3) where 0-cm in-situ top-ground temperature measurements were available, we finally preserved 2107 stations characterized by $r_{clr} > 0.9$. In the subsequent step, remote sensing LST under cloud and under clear-sky conditions were respectively validated at these stations, with the results revealed in [Fig. 3](#). It is manifested through [Fig. 3\(a\)](#) and [3\(b\)](#) that very close performances have been achieved between the clear-sky and the cloudy scenarios, especially considering their almost equally high validating correlations between 0.94-0.96. For each independent station, we calculated the “RMSD difference (RMSD_diff)” between the two scenarios, based on the formula of “ $RMSD_{clr} - RMSD_{cld}$ (the subscripts of ‘*clr*’ and ‘*cld*’ denote clear-sky and cloudy conditions separately)”. The statistical distribution of this RMSD difference with regard to different stations is shown in [Fig. 3\(c\)](#). Apparently, 1942 stations all over the country have obtained an RMSD difference value below 2.6 K, and the mean RMSD difference is [only](#) about 1.9 K. All above results have indicated that the uncertainty of our night-time LST reconstruction algorithm proposed for cloudy conditions is not very significant. The corresponsive uncertainty that could be propagated to downscaled SSM in this stage is analyzed below in Section 3.2.



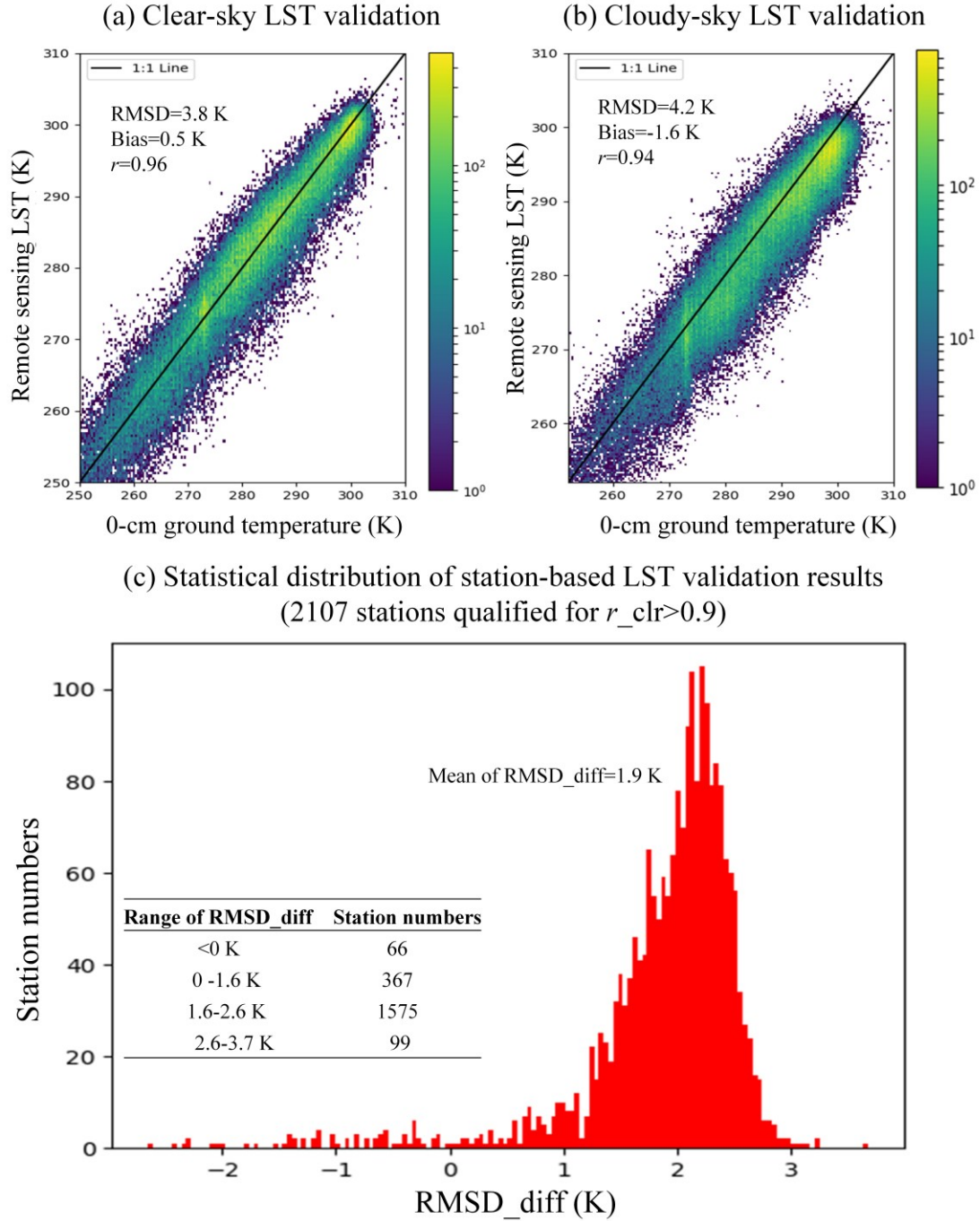


Fig. 3 validation results of the cloud gap-filled LST in China. (a) Density plot of thermal infrared LST under clear-sky condition compared to the 0-cm ground temperature measurements for all stations. (b) Same to (a) but for thermal infrared LST under cloudy conditions. (c) Statistical distribution of difference between RMSD of clear-sky LST and RMSD of gap-filled LST under cloudy condition with regard to different meteorological stations over the study region.

3.2 Evaluation on the final 1-km SSM product

The overall validation results of the finally downscaled 1-km SSM product is demonstrated in [Fig. 4](#). [Fig. 4](#)(a) shows that about 85% (N: 1833) of the total 2154 stations (the remaining 263 stations are located in pixels with no effective PM observations and are thus removed) have obtained significantly positive downscaling gains ($G_{down} > 0.03$). This hints that the 1-km SSM product can better capture the dynamic behaviors of local ground soil moisture data than the original 36-km PM NN-SM data, revealing higher spatial representativeness of the downscaled SSM data product over the country. According to [Fig. 4](#)(b), the mean ubRMSD of all stations is about 0.054 vol/vol, while 90% of those stations have the number lower than 0.088 vol/vol. In addition, we made another analysis concerning the possible influence of land cover types on SSM downscaling performance in [Fig. 4](#)(c). The spatial information of land cover types was derived from the MODIS MCD12Q1 ([10.5067/MODIS/MCD12Q1.006](https://www.modisweb.org/modisweb/view.do?dataset=10.5067/MODIS/MCD12Q1.006)) IGBP-based land use image in 2019. For stations that experienced land use change throughout the years of the study period, the ubRMSD is only reported for data in the year of 2019. Clearly, better accuracies are observed mainly in grassland, cropland and bare soil surface, whilst relatively poorer performances (with averages of ubRMSD higher than 0.06 vol/vol) are seen in urban regions, (woody) savanna, and crop-to-natural-vegetation mosaic areas. Such a relative performance across land covers is logical because all the land cover types with their average ubRMSD higher than 0.06 vol/vol are characterized by lower hydrologic

491 homogeneity in terms of their definition, e.g. savanna, which is a mixture of grass and
492 tall trees, and urban areas, which are composed of impervious underlying surface.

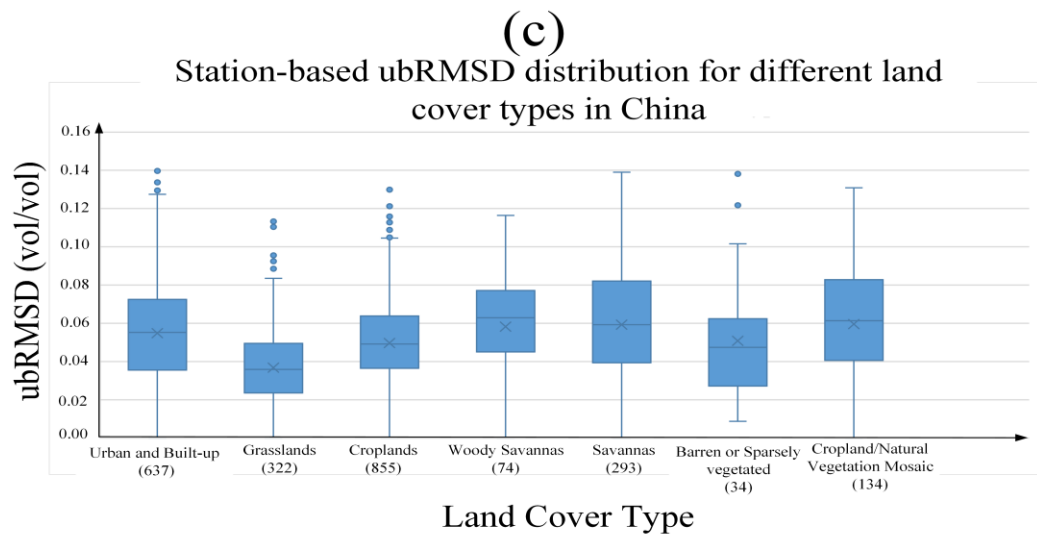
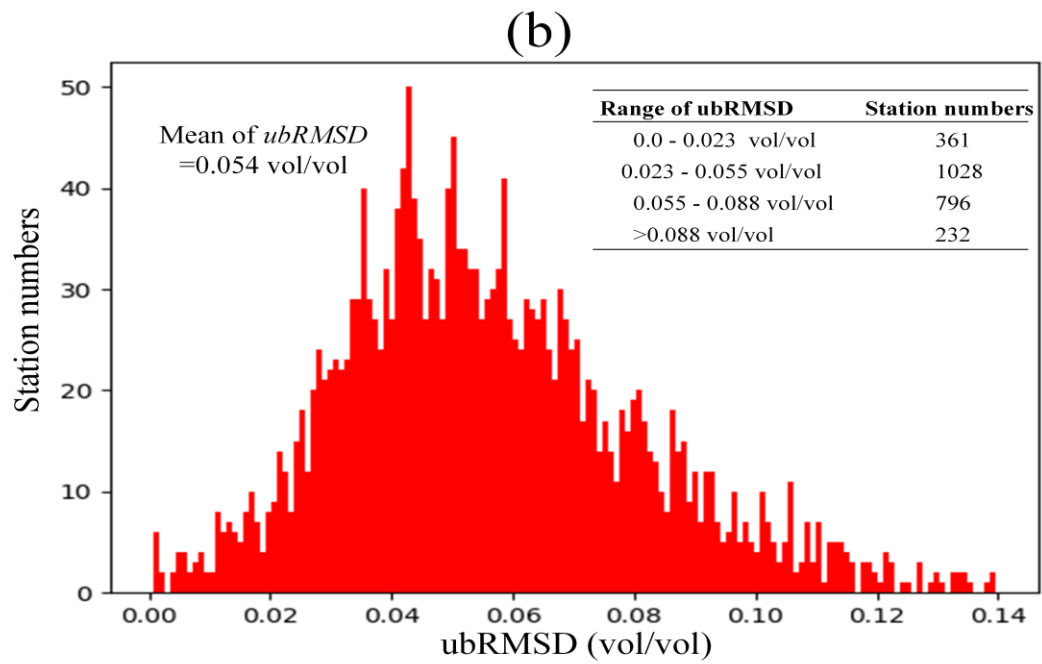
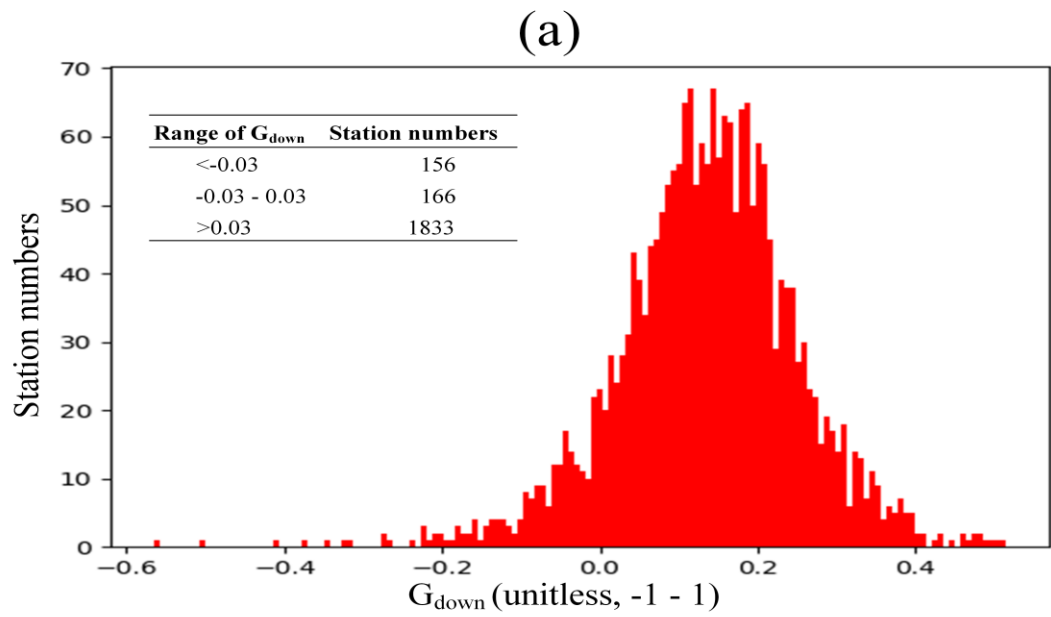
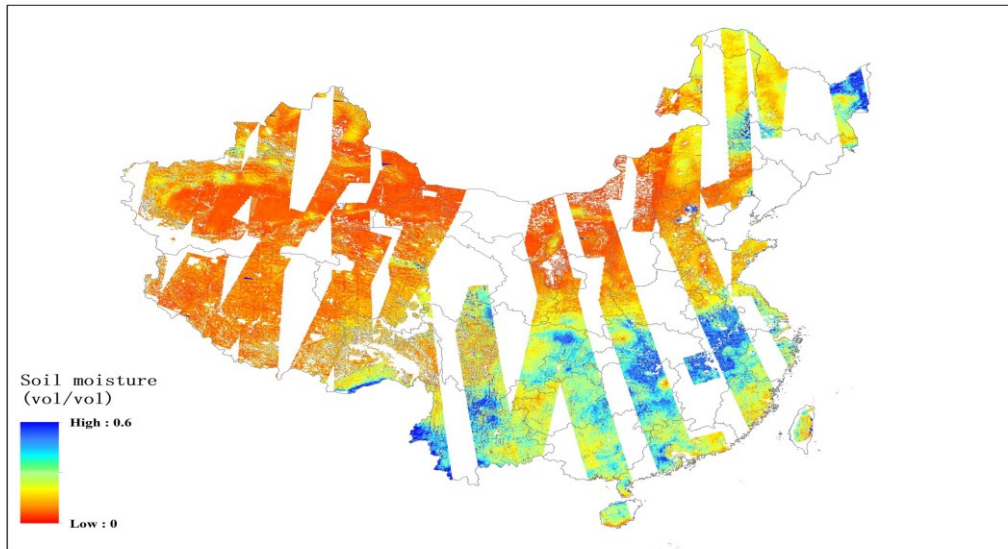


Fig. 4 General validation results of the currently developed SSM product. (a) G_{down} distribution for different stations over China. (b) ubRMSD distribution for different stations over China. (c) ubRMSD statistics reported for different land covers. The numbers in the parentheses of the x-axis labels represent the amount of meteorological stations corresponding to that specific land cover type.

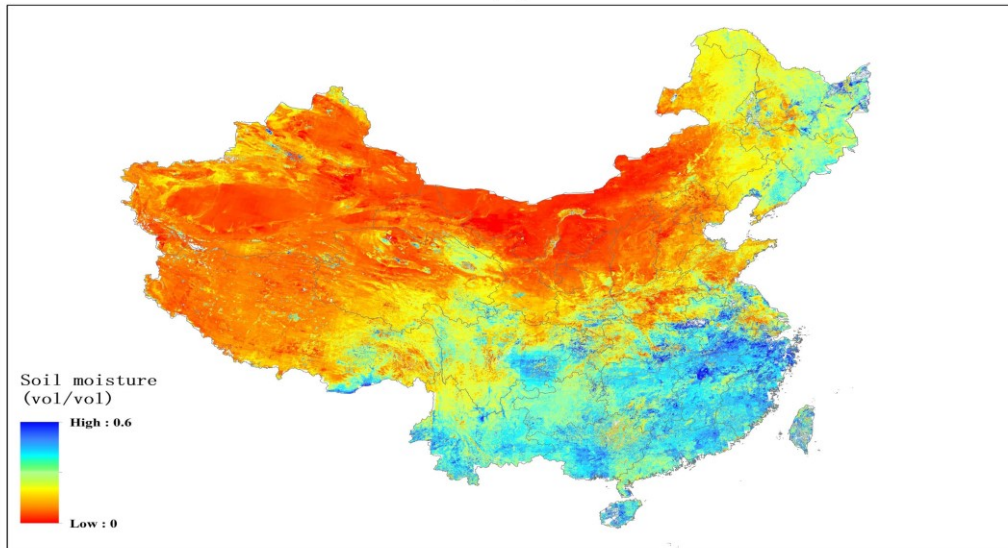
In [Fig. 5](#) (b) we employed the downscaled SSM image on April 9, 2018, as an example to demonstrate the spatial features of the developed product. Meanwhile, we also show the map of SMAP/Sentinel combined SSM (SPL2SMAP_S_V3) obtained from April 6 to April 11, 2018 in [Fig. 5](#) (a), as a contemporaneous comparison reference. Clearly, the SPL2SMAP_S_V3 map has a much lower coverage percentage over the study region compared with the map of the currently developed product on one single date, even though the former was generated based on multi-date images. Both maps show similar spatial texture depicting the relatively dry climate in northwestern China compared with the humid climate in the Middle-lower Yangtze River Plain. Nevertheless, there also exist cases where the details in texture differ prominently, like that in the far northeastern end of the country. For the sake of further analysis on this point, results of the quantitative comparison as proposed in Section 2.1.4, is demonstrated in [Fig. 5](#) (c) and [Fig. 5](#) (d). The currently developed SSM product obtained a 0.078 vol/vol ubRMSD and a correlation coefficient of 0.55 against the in-situ soil moisture measurements, converging more apparently to the 1:1 line when compared with validation result of the SPL2SMAP_S_V3 dataset. As with the area of China, therefore, the currently developed product is superior to the global

515 SMAP/Sentinel combined SSM in terms of both coverage percentage and estimate
516 accuracy.

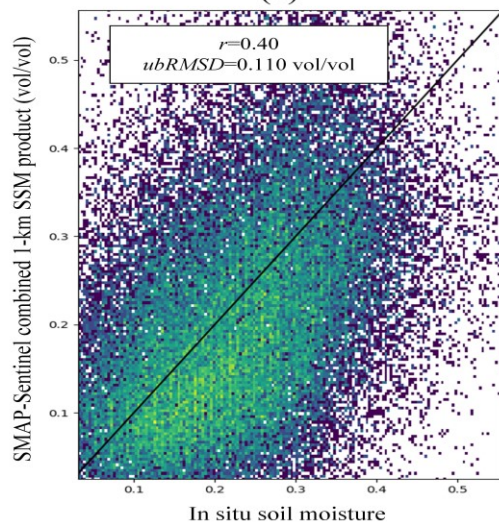
(a)



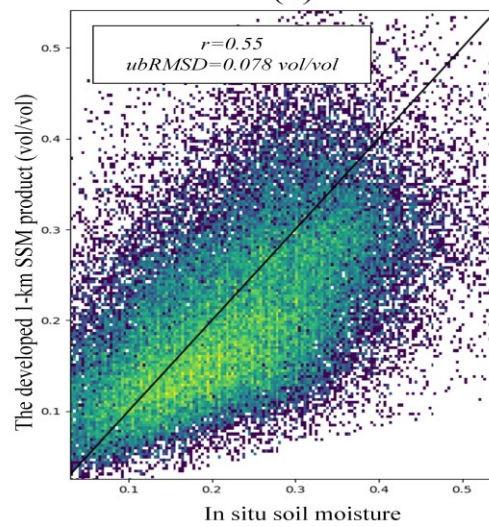
(b)



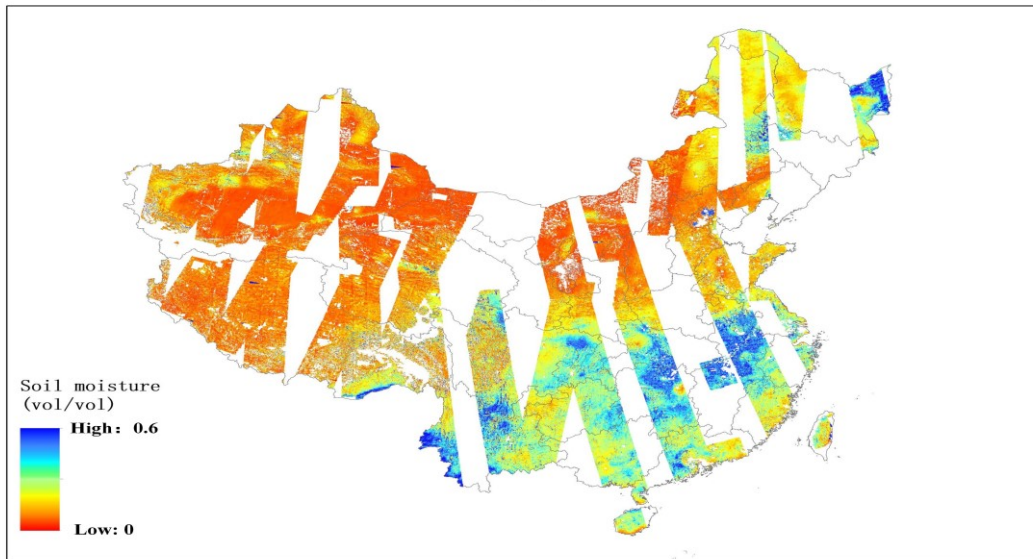
(c)



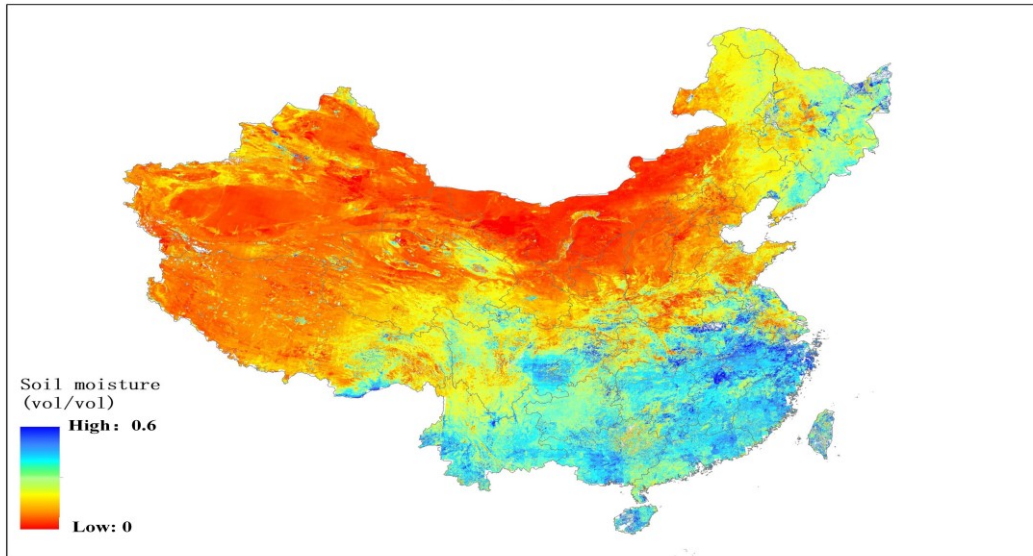
(d)



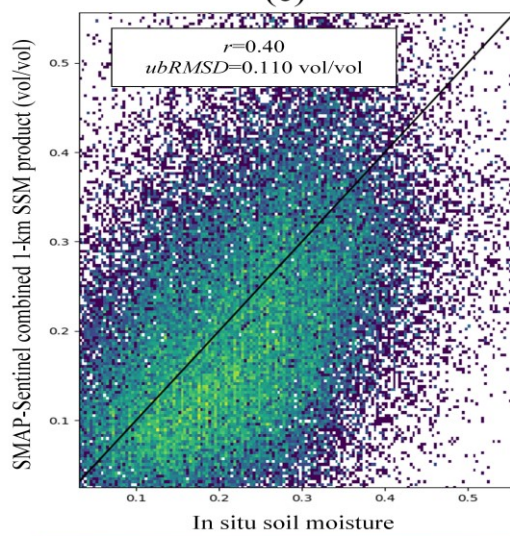
(a)



(b)



(c)



(d)

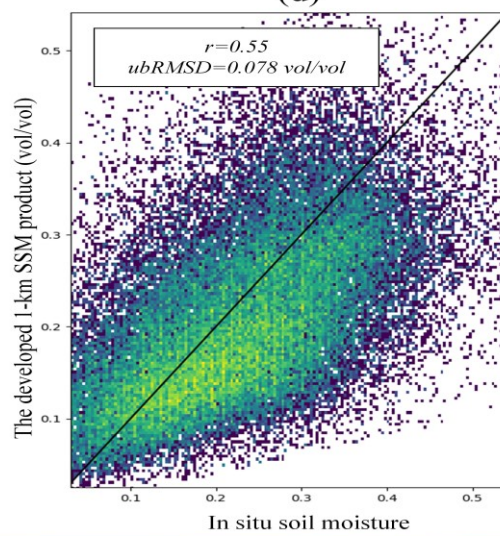
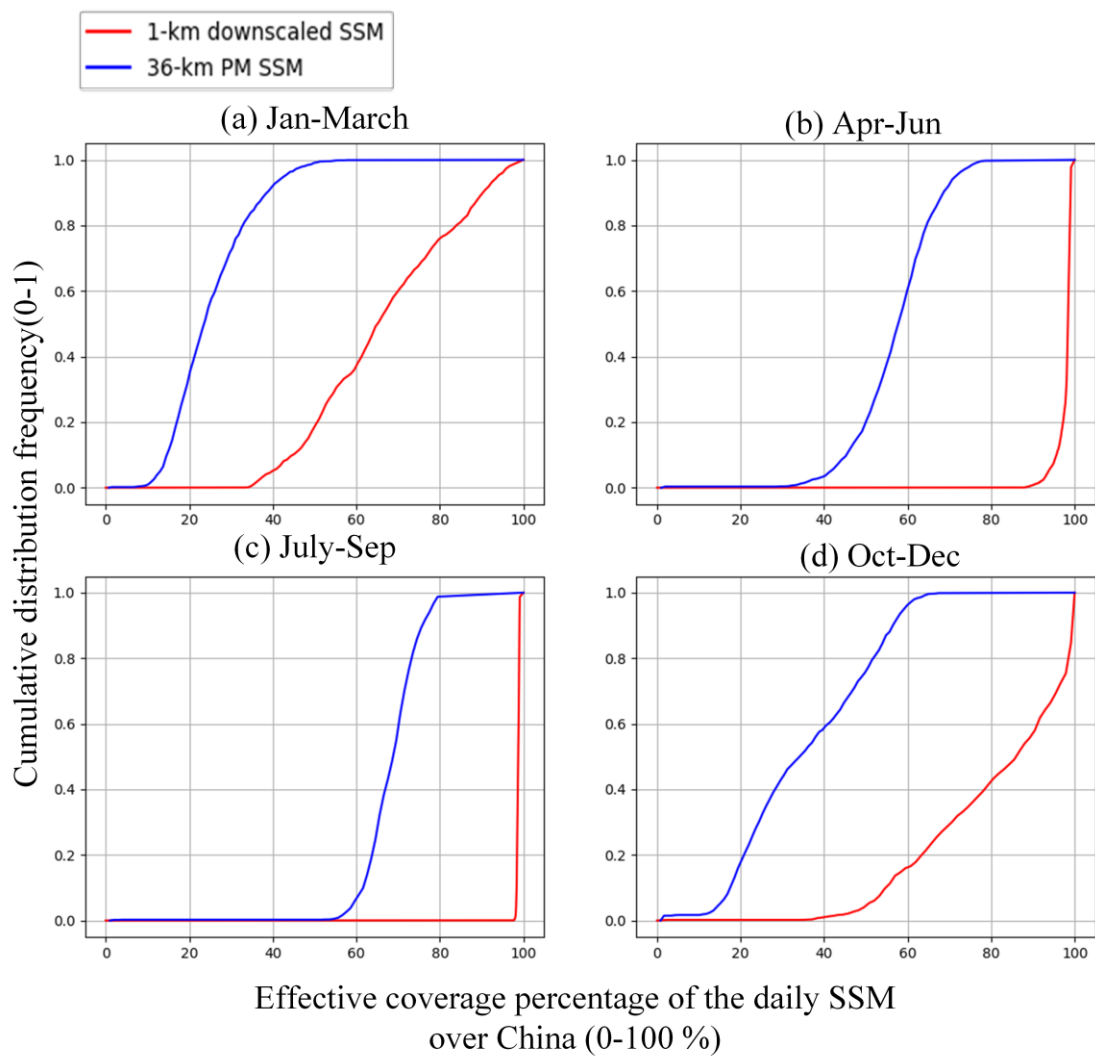


Fig. 5 Comparison results between the currently developed 1-km SSM product and the SMAP/Sentinel combined 1-km SSM (SPL2SMAP_S_V3). (a) SPL2SMAP_S_V3 SSM images over China at about 6:00 a.m. synthesized by 6 continuous dates from April 6, 2018 to April 11, 2018. (b) The SSM image at 1:30 a.m. of April 9, 2018 from the currently developed product. (c) Validation results of the SPL2SMAP_S_V3 product against in-situ soil moisture measurements over China for years of 2017, 2018, and 2019. The black solid line is the 1:1 line. (d) Same to (c) but for validation of the currently developed SSM product.

In [Fig. 6](#), we display the cumulative distribution frequency of coverage percentages of the downscaled SSM product and of the original PM NN-SM product for each season. We should be noted that in this statistical scheme, pixels identified as static water body by the MODIS MCD12Q1 land cover type product were not considered in the denominator of the coverage percentage. Besides, the gap time between the respective on-orbit period of AMSR-E and of AMSR-2 (from October 2011 to June 2012, during which there are no effective observations from the PM NN-SM product) were also excluded. It is apparent that in [Fig. 6](#)-(b) and -(c), almost all downscaled daily SSM images over the 16-17 years have achieved a coverage percentage ~~close to 100% (at least above 95%)~~ [higher than 85%](#). In comparison, the majority of the PM NN-SM daily images have their coverage percentages below 80% over the study region, primarily due to the PM-seam gaps particularly existing in low latitudes (see Section 2.2.2). In [Fig. 6](#)-(a) and -(d), the percentages of effective pixels in both the PM and the downscaled SSM images are far lower than their counterparts in the other two subfigures. This is mainly ascribed to extreme

541 meteorological conditions including snow, ice, and frozen soils that are typically
542 persistent throughout most of these specified months in the northwestern regions of
543 China. Such conditions can impede reliable estimates of SSM based on all satellite
544 remote sensing techniques in the current time. [The above inter-seasonal differences on](#)
545 [data coverage are also reflected in Fig. 7 in another manner based on presenting the](#)
546 [spatial distributions of number percentages of available dates in each three-month](#)
547 [period.](#)



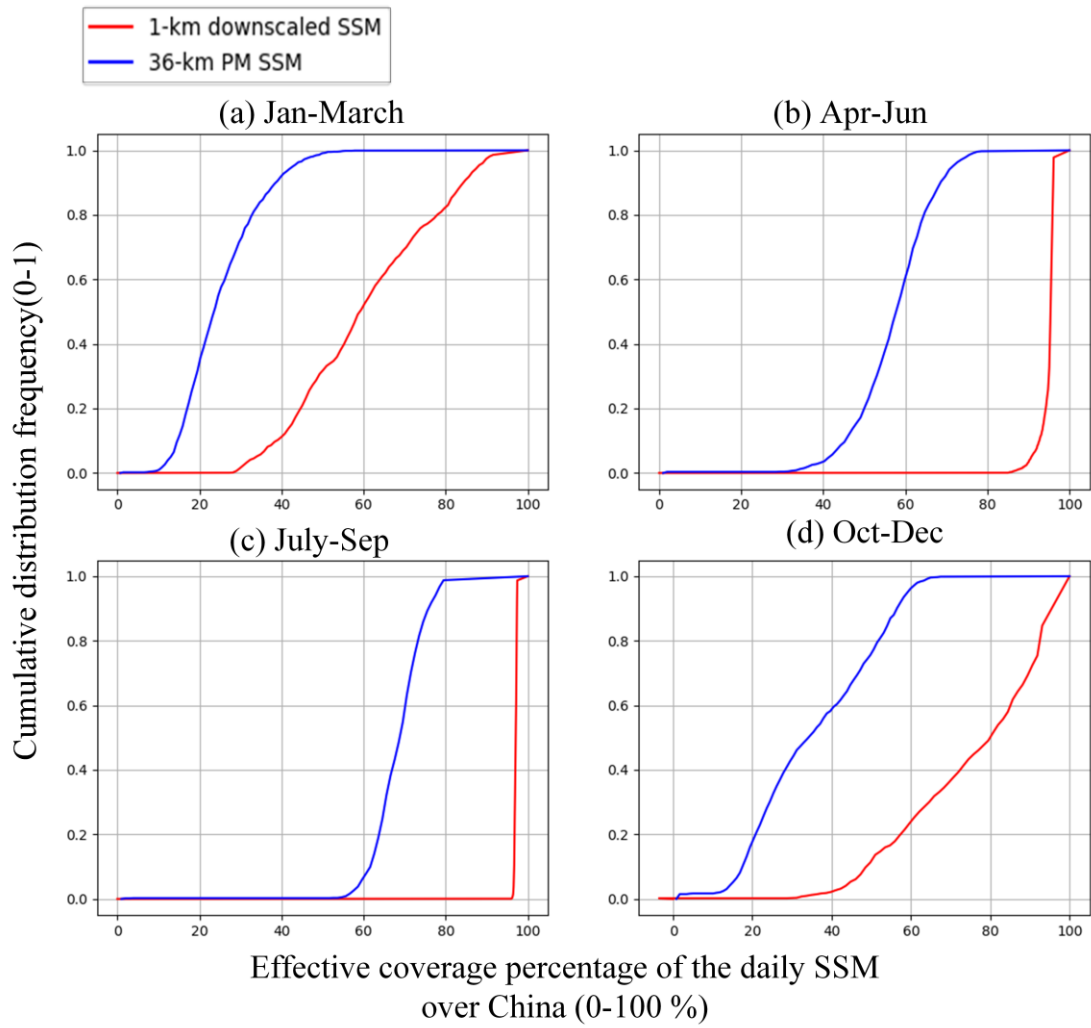
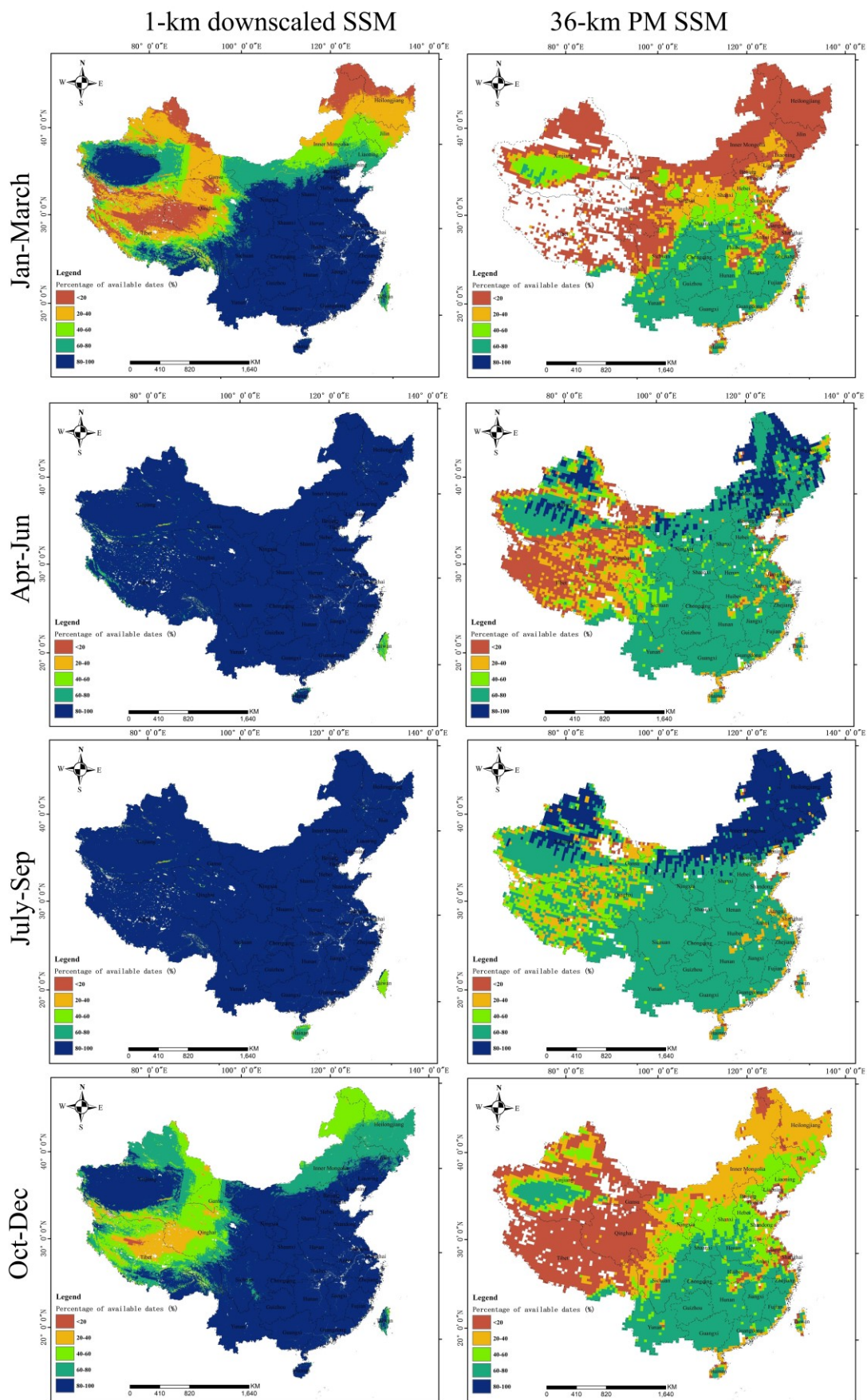


Fig. 6 Cumulative distribution frequency of our proposed SSM product against the original 36-km SSM product for different seasons. The period between October 2011 and June 2012 is excluded in the current statistics.



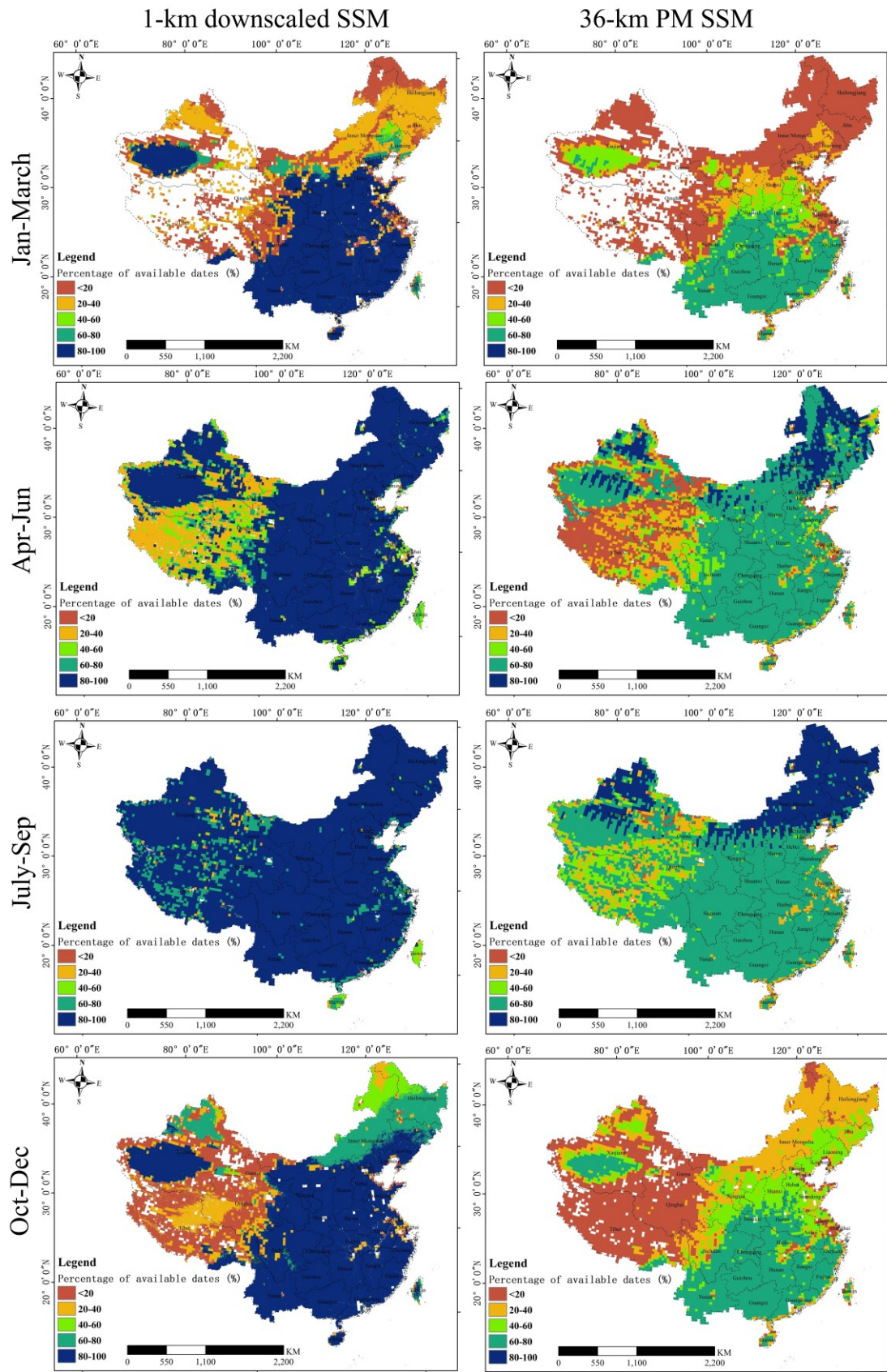


Fig. 7 Spatial distributions on percentage of day numbers with available estimates for the currently developed 1-km SSM product and the original 36-km PM data during 2003-2019. The four different

periods (i.e., January-March, April-June, July-September, October-December) of a year are treated respectively. The period between October 2011 and June 2012 is excluded.

The techniques behind coverage improvement of the downscaled SSM (against PM and optical data inputs) can be categorized into two classes, i.e. cloud gap-filling of the input optical datasets (see Section 2.2.1), as well as the filling of downscaled SSM in PM-seam gaps (see Section 2.2.2). [Table 2](#) reports the specific validation results (using averages of all stations) of downscaled SSM in these coverage-improved conditions, relative to that generated without using any coverage improvement technique, in order to evaluate the propagated effect of such techniques on the final product. The very limited difference for ubRMSD values (0.053 vol/vol versus 0.056 vol/vol) between cloudy and clear-sky conditions suggest that the [1-km SSM estimates from our final product are cloud-gap-filling techniques are](#) generally compatible [with SSM downscaling between cloudy and clear-sky conditions](#). [To a certain extent, our pre-assumption that the theoretically hypothesized ‘clear-sky’ LST reconstruction is proved suitable for quantifying soil wetness variation.](#) The downscaled SSM estimated for regions of PM-seam gaps have a slightly worse (but still acceptable) accuracy, considering its ubRMSD of 0.059 vol/vol compared to the 0.052 vol/vol ubRMSD of the PM-observed 1-km pixels. In summary of [Fig. 6](#) and [Table 2](#), the currently developed product has achieved a substantially improved spatial coverage against the original remote sensing input datasets, whilst successfully preserved the SSM downscaling accuracy of the observation-covered pixels at the same time.

Table 2 Comparisons between validation results for pixels under coverage-improved regions and

for pixels under remote-sensing-observation-covered regions.

Evaluation metric [*]	Comparison between cloudy and clear-sky conditions		Comparison between passive microwave (PM) observed regions and regions of PM-seam gaps	
	Clear-sky condition	Cloudy condition	PM-observed regions	PM-seam gaps
ubRMSD (vol/vol)	0.053	0.056	0.052	0.059
Correlation coefficient	0.49	0.47	0.49	0.44

*All evaluation metrics in this column indicate the average of all available stations

4. Discussion

4.1 Uncertainty on SSM evaluation between satellite- and ground- scales

In this study, we made evaluations on remote sensing SSM products at different spatial resolutions, using measurements from 2000+ stations provided by the national-level soil moisture observation network of China as standard benchmark. Through the evaluations, a ubRMSD of 0.074 vol/vol is reported for the original 36-km NN-SM SSM product (Fig.A1-b). We notice that this result is considerably poorer if compared with another previous evaluation campaign targeting at the same product (Yao et al., 2021), which achieved a global RMSE (RMSD) of 0.029 vol/vol. However, this difference is not unexpected because the two campaigns were carried out in different regions of the world. Also, that particular study (Yao et al., 2021) was conducted based on completely different ground soil moisture observations provided by the International

Soil Moisture Network (ISMN) (Dorigo et al., 2021). Compared to the observation network employed in this study, the observation sites of ISMN are more intensively distributed as an “integrated soil moisture station” so as to provide spatially average soil moisture within a grid of tens of kilometers. In this regard, we admit that the ISMN is generally more professional in evaluating satellite PM-based SSM retrievals at a coarser resolution. But on the other hand, only a few (≤ 4) of such “integrated stations” have been set up sporadically within China, making the ISMN data much less representative of our study region compared with the national-level soil moisture network of China exploited by our current study.

Although the higher RMSD of the national-level soil moisture network of China may indicate larger measurement uncertainty than the ISMN, the negative influence that might be imposed on our study purpose should be inconsequential. This is because we focus more on the relative validation performance of different SSM products, rather than on the absolute value of any evaluation metric including ubRMSD and correlation coefficient calculated against ground measurements. Specifically, the 1-km downscaled SSM obtained an average ubRMSD of about 0.054 vol/vol among different stations according to [Fig. 4](#)(b). Besides, result of the evaluation in [Fig. 5](#)(d) based on combination of multi-station ground measurements shows a global ubRMSD of 0.078 vol/vol for this product. Overall, the above-mentioned results can be identified as at least comparable to the global (multi-station based) ubRMSD of 0.074 vol/vol of the original NN-SM data as they are evaluated against the same benchmark. Therefore, conclusion is safely drawn that the currently developed product preserves the retrieval

accuracy of the coarse-resolution NN-SM data, whilst improving the spatial representativeness of the latter product substantially according to the mostly positive G_{down} values in Fig. 4(a).

Moreover, one may also argue that the r -value of 0.55 for the currently developed product in Fig. 5(d) is not sufficiently high compared with several previous studies (Wei et al., 2019; Sabaghy et al., 2020) obtaining r -values above 0.7 for temporal analysis of satellite remote sensing soil moisture. However, we should be noticed that these previous studies have conducted analyses respectively at the temporal and the spatial dimensions. Based on their results, the spatial analysis typically derived lower r -values (<0.4) compared to that at the temporal dimension. This is probably because the heterogeneity degree of remote sensing pixels can vary significantly across different sites. Since the evaluation in Fig. 5(d) was deployed at the ‘spatio-temporal’ integrated dimensions, such an r -value is expected. This is also close to the global r -value of 0.6 for validation of the coarse-resolution NN-SM product as reported in Yao et al. (2021).

4.2 Uncertainty on cloud gap-filling and validations of LST

~~As has been mentioned in Section 2.2.1, we utilized LST gap-filled based on the STDF method was used alone as one of the main input datasets for SSM downscaling under cloudy weather. Although such LST inputs contain clear-sky bias from the real cloudy condition, it is found to performs better in driving the SSM downscaling model compared with its bias-adjusted counterpart (see Section Appendix-B for details). The reason may be linked to one of the basic theories behind our SSM downscaling~~

methodology, i.e. the “universal triangle feature space (UTFS)” theory (Carlson et al., 1994). In the UTFS, clear-sky LST is employed to implicitly quantify the surface soil wetness degree as it correlates with the dynamics of soil evaporative efficiency and soil thermal inertia when vegetation cover density is fixed. Under cloudy conditions, however, the satellite observed LST ~~would be a proxy of~~ is subjected to not only surface soil property, but also to that related to cloud insulation effect from solar incoming radiation and ground long wave outgoing radiation. As a result, the actual relationship between SSM and cloudy LST could be much more complicated than the one that has been described by the UTFS-based SSM downscaling model (i.e. Equation-2). In comparison, LST generated by the STDF alone for assumed clear-sky conditions, as is free from interference of cloud, would be a comparatively more competent input variable for driving the UTFS-based SSM downscaling model under non-rainy clouds. This is especially the case for thin and short-time clouds with marginal direct feedbacks on surface soil wetness.

However, we admit that ~~when rainy clouds occur,~~ the STDF-filled LST ~~under rainy clouds~~ is also not suitable for our study purpose. This may explain the slightly higher RMSD for SSM under cloud based on STDF-filled LST (0.056 vol/vol) compared to that under real clear sky (0.053 vol/vol), as shown in Table 2. In reality, the actual negative influence of cloud on the final SSM product may be even more serious than ~~indication from~~ the above RMSD difference (i.e. $0.056 - 0.053 = 0.003$ vol/vol) ~~has shown~~, due to the portion of “clear/cloudy-weather-mixed” spatial windows during the fitting process of the downscaling model. In these windows, uncertainty in cloud gap-

filled LST may affect accuracy of the fitted model coefficients and thus deteriorate the final SSM estimates in clear-sky pixels within the same window. Consequently, the above RMSD difference has been more or less underestimated. Despite all of above, in our study area of China we regard the STDF-filled LST as a more optimal proxy of heat flux for estimating SSM under clouds, compared to the bias-adjusted LST. On the other hand, future efforts are encouraged to further clarify the mechanical relationships between STDF-filled/bias-adjusted LST and soil wetness degree under clouds.

Different from a number of previous studies (Jiménez et al., 2017; Dowling et al., 2021; Yang et al., 2019) validating satellite thermal-infrared-based LST based on longwave radiation observations made at footprint-level observation stations (e.g. flux towers), our study has used 0-cm top ground temperatures as the primary benchmark for this validation campaign instead. Similar to that for SSM validation, the most crucial motivation driving such an experimental design is the significantly intensive distribution of the meteorological stations compared to the very limited number of active and effective flux towers available in China. It is noted that these measurement devices at all of the meteorological stations are required to have been instrumented under open environmental conditions with relatively lower fraction of tall trees and water bodies, in order to conduct efficient monitoring at the physics of near-surface air. This can also be reflected in Fig.4-(c), which reveals no stations built within forest covers. Moreover, as we only focus on the mid-night scenario when the states of all land observations are “most stable” during one diurnal cycle, uncertainties due to the possible temperature inconsistency between bare ground surface and high tree surface

as well as due to the temporal mismatch (from about 1:30 to 2:00 A.M.) should have minimalmargional effect on our results. We have carried an extra test that can confirm this discussion, with the detailed procedures described in Section Appendix-C. Wang and Liang (2009)

4.3.2 Major novelty, unique profit, and future prospect of the developed product

Compared with the widely known active/passive microwave combined SSM product (e.g. the SPL2SMAP_S_V3) and other PM/optical-data combined counterparts which were also published recently but at the monthly scale (Meng et al., 2021), the major novelty of the currently developed product mainly lies in the fact that it has achieved progress on all of the three crucial dimensions of satellite remote sensing, including the temporal revisit cycle (daily), the spatial resolution (1-km), and the quasi-complete coverage under all-weather conditions. To our knowledge, this has rarely been achieved by previously developed satellite soil moisture product at regional scales. For realization of the above-mentioned progresses, we have fused the SSM downscaling framework with other techniques including cloud gap-filling of thermal infrared LST, MWS-based temporal filtering of vegetation indices, as well as reconstruction of seams between neighboring PM swaths in low latitudes. The final SSM estimates under cloudy conditions and intersected with the PM-seam gaps were specially validated against the rest estimates under clear sky and in the regions covered by PM observations, respectively (Table 2Table 2). The comparable performances among all treatment

groups herein confirm that the accuracy of the product is stable and consistent among all weather conditions.

With improvement achieved at the three dimensions, unique profit of the currently developed product can be taken by subsequent studies and various industrial applications. For example, the capability of this product can be investigated on capturing the short-term anomaly of local hydrological signals as well as improved monitoring on drought disasters, which used to be investigated mainly at a coarser resolution by PM SSM (Scaini et al., 2015; Champagne et al., 2011; Albergel et al., 2012). For another, taking advantage of its all-weather daily time series, the product can be utilized together with precipitation data to isolate and quantify the anthropic influence on regional water resources from the natural hydrological dynamics. Examples of such anthropic signals include agricultural irrigation activities, as well as finer-scale information on agricultural crops which was previously interpreted based on PM-driven techniques (Song et al., 2018). In addition, we should realize the important role of soil moisture as a constraint for accurate estimation of surface evapotranspiration and runoff (Zhang et al., 2020; Zhang et al., 2019). Therefore, the profit of this product can be further enhanced if coupled with land-atmosphere coupled models to produce new insights into water-cycle processes of earth surface at a finer spatio-temporal scale.

In the future, the methodological framework proposed in this paper is prospective to be universally applied in other regions of the world to serve for better monitoring of the global surface wetness in the following studies. If applied in continental and global

scales, however, the current process for gap-filling of PM seams may require further attention and improvement. In this study, SSM in regions intersected with PM-seam gaps were estimated using TB observations from PM swaths at neighboring dates (see Equation-5). Although the errors in the PM-seam gaps over China as reported by [Table 2](#) are only slightly larger compared to the PM-covered regions, they cannot be ignorable completely and may leave extra concern on the universality of this technique, especially in the low latitudinal tropical regions where the effect of PM-seam gap is more apparent than in our study area. Besides, another imperfection of this data product lies in the gap period between AMSR-E and AMSR-2. Considering the different systematic error patterns of various PM SSM products, we did not generate downscaled SSM based on other PM products (e.g. the SMOS SSM product) during this period but just left the period as null values. We suggest a more rigorous and universal inter-calibration framework on different PM SSM products to be developed in the future for a long-term consistent 1-km downscaled SSM dataset.

5. Conclusions

This paper describes the main technical procedures of a recently developed remote sensing surface soil moisture (SSM) product over China covering the recent ten years and more. Based on combination of passive microwave SSM downscaling theory and other related remote sensing techniques, the product achieves multi-dimensional distinctive features including 1-km resolution, daily revisit cycle, and quasi-complete all-weather coverage. These were rarely satisfied completely by other existing remote

sensing SSM product at regional scales. Validations were conducted against measurements from 2000+ automatic soil moisture observation stations over China. Overall, an average ubRMS~~DE~~ of 0.054 vol/vol across different stations is reported for the currently developed product. The mostly positive G_{down} values show this product has significantly improved spatial representativeness against the 36-km PM SSM data (a major source for downscaling). Meanwhile, it generally preserves the retrieval accuracy of the 36-km data product. Moreover, additional validation results show that the currently developed product surpasses the widely used SMAP-sentinel combined global 1-km SSM product, with a correlation coefficient of 0.55 achieved against that of 0.40 for the latter product. The methodological framework for product generation is promising to be applied at the continental and global scales in the future, and the product is potential to benefit various research/industrial fields related to hydrological processes and water resource management.

Appendix

A. Evaluation on different PM SSM products

We have made evaluations on the various AMSR-based SSM products (as shown in [Table 1](#)~~Table 1~~) covering the recent 10 years or longer, based on our soil moisture observation network all over China. The L-band based SMAP SSM dataset was also evaluated as a reference. The evaluation period covers the three years of 2017, 2018, and 2019. All AMSR-based 25-km grids were re-set to the SMAP 36-km grid system using the nearest resampling method. Only grids that contain equal or more than 4 soil moisture measurement stations were employed, in which, the grid-based PM SSM estimate was compared with average of measurements from all interior stations. Finally, 53 grids were selected, as shown by the green color in Fig.A1-(g). For AMSR-based products, only the mid-night descending datasets were evaluated, whilst for the SMAP product, our evaluation only focused on its descending mode in the early morning.

As manifested by Fig.A1-(a) to -(f), the selected SSM product in the current study, i.e., the NN-SM product has an unbiased RMSD of 0.074 vol/vol and a correlation coefficient of 0.49. This obviously outperforms the other three traditional AMSR-based SSM products (i.e. JAXA-AMSR, LPRM-AMSR, and UMT-AMSR products) and is only inferior to the SMAP SSM retrievals, whilst the later only covers the latest period since 2015. As far as CCI data are concerned, it has a similar performance against the selected NN-SM in general. Nevertheless, the region marked by red circle in Fig.A1-(c) indicates that CCI estimates have a considerably larger proportion of overestimated

783 anomalies. But overall, the primary reason that we have abandoned CCI but selected
784 NN-SM is because the latter can provide a higher coverage fraction of valid pixels in
785 our study region, as has been stated in Section 2.1.1.

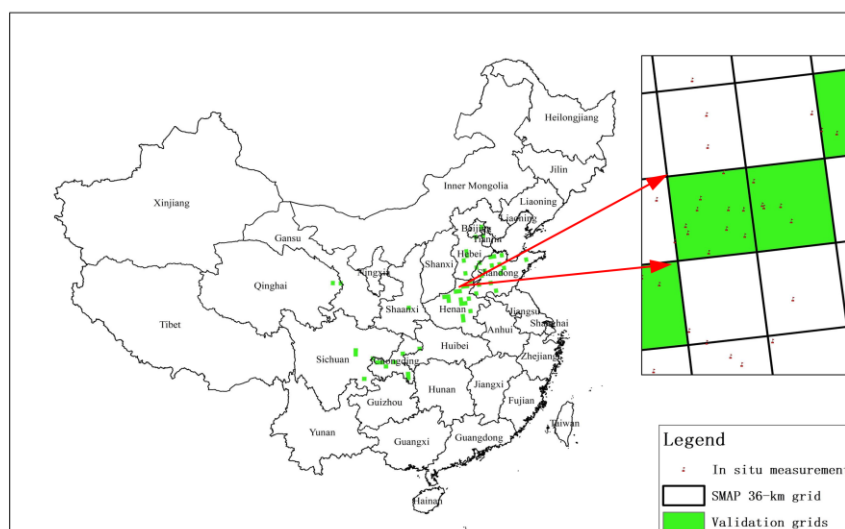
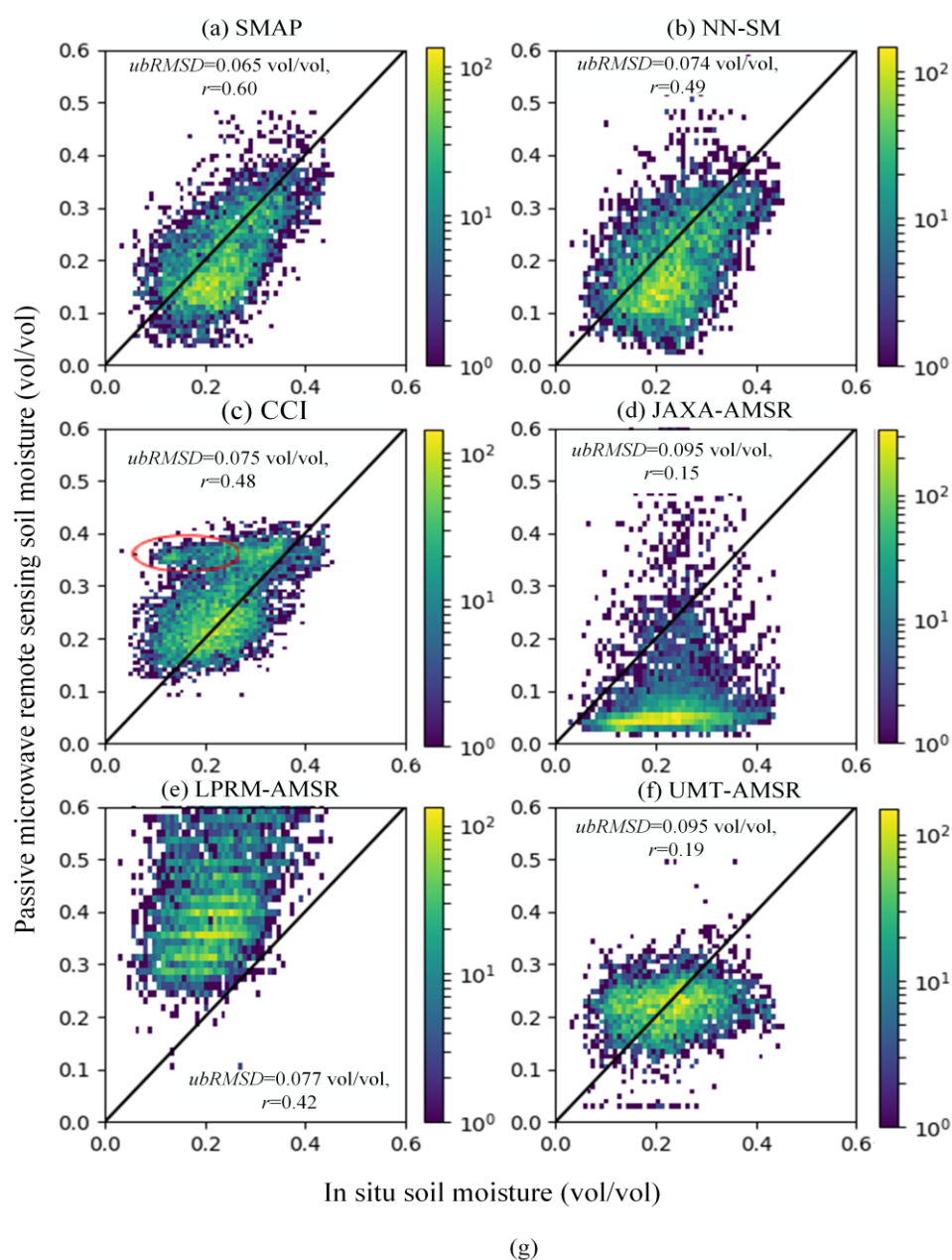


Fig. A1 (a)-(f) Comparison of different PM SSM products (as reported in [Table 1](#)) against the in situ SSM measurements in China. (g) Locations of the 36-km EASE-GRID-projection based pixels used for this comparison campaign.

B. Evaluation on the influence of bias adjustment for reconstructed ‘clear-sky’ LST under cloud

In Section 2.2.2, we have emphasized that the gap-filled LST for cloudy pixels reflects the theoretical surface temperature of that pixel under a hypothetical clear-sky condition. As this cloud gap-filled LST would suffer from a possible bias against the real surface temperature under cloud (Dowling et al., 2021), we made an additional experiment regarding to further improvement of this cloud gap-filled LST. The follow-up step for bias adjustment of this hypothetical clear-sky LST (but actually under cloudy conditions), as expounded in Section 4.2 of Dowling et al. (2021), was conducted herein using remote sensing and in situ LST data over China but only in 2018. We illustrate the validation results for bias adjusted and non-bias adjusted LST under cloudy conditions in Fig. A2-(b) and -(c), respectively. Similar to [Fig. 3](#), validation results for clear-sky LST of that year are also displayed (Fig. A2-(a)) for comparison. The results generally show that the follow-up step is effective in reducing the bias of the originally gap-filled ‘clear-sky LST’ under cloudy conditions (from -1.7 K to 0.4 K).

In the subsequent step, we substituted the original non-bias adjusted LST under cloudy conditions with its bias adjusted counterpart, and used the latter as the input for SSM downscaling. The general validation results of the downscaled SSM are illustrated

in Fig. A3 (similar to that presented in [Fig. 4](#)~~Fig. 4~~-a and -b). Contrary to the above-analyzed Fig. A2, the bias adjusted cloudy LST with better gap-filling accuracies, however, obtained inferior performance in SSM downscaling. This final validation result, to some degree, confirms our assumption in Section 2.2.2 that the reconstructed cloudy LST but for the hypothesized clear-sky condition is the better proxy of surface moisture dynamics. But overall, as all LST estimates discussed herein are for the midnight scenario (when the energy interaction between atmosphere and land surface is relatively weak), the RMSD difference for different weather conditions in Fig.A2 is expectedly marginal. As a consequence, the difference in ubRMSD of SSM in Fig.A3 can hardly be identified as ‘very significant’. Therefore, we encourage further tests on this conclusion in specific future studies to confirm its universality, especially for situation of the ‘morning to noon’ time window.

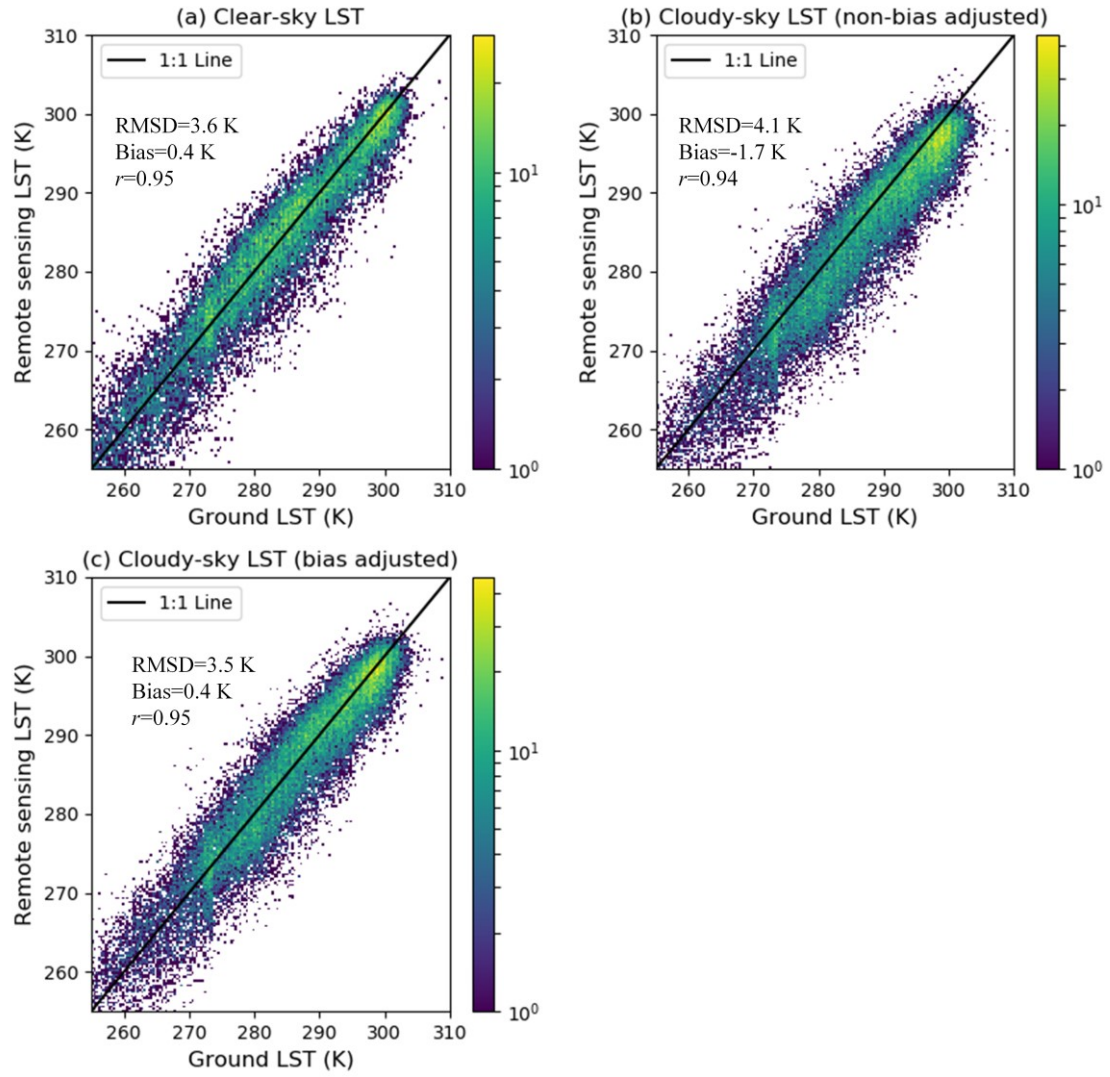


Fig. A2 Validation of the clear sky LST (a), reconstructed LST under cloud but with no passive-microwave based bias adjustment (b), as well as the reconstructed LST under cloud with passive-microwave based bias adjustment (c) respectively, based on the 0-cm ground temperature measurements at meteorological stations.

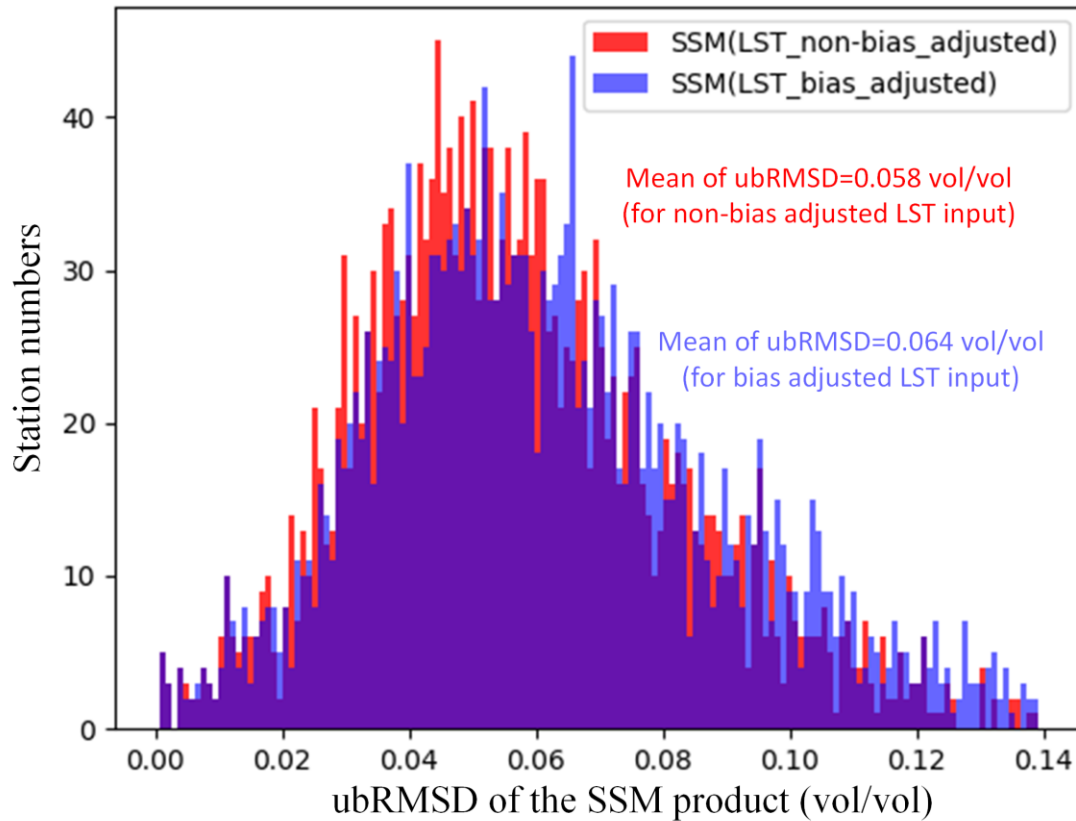


Fig. A3 The statistical distribution of ubRMSD at different stations for SSM estimates driven by two
respective kinds of cloudy LST inputs.

C. Uncertainty test between 0-cm ground temperature observations and flux-tower-derived thermal infrared LST

We herein utilized 4 flux towers to calculate their footprint-level (about 500-1000 m) thermal infrared LST based on long wave radiation measurements, plus broad band emissivity data derived from the MODIS MYD21A1 product (MYD21A1N.V061). The 4 towers are all characterized by moderate or low vegetation (grassland) and are dispersedly located at different eco-regions of China, namely the towers of Changling, Huailai, Yakou, and Naqu (see the inset map in Fig.A4-b). Data from Changling are derived from the FLUXNET community (FLUXNET2015 Dataset - FLUXNET) in 2010.

[Data from the other three towers are derived from the National Tibetan Plateau Data Center, with data DOIs of <http://dx.doi.org/10.11888/Meteoro.tpd.c.271094> for Huailai in 2018, <http://dx.doi.org/10.11888/Meteoro.tpd.c.270781> for Yakou in 2018, and <http://dx.doi.org/10.11888/Meteoro.tpd.c.270910> for Naqu in 2016. These data have been preprocessed by their providers to record the dynamics of those variables at a half-hour interval. The algorithm for calculating LST based on flux-tower-derived long wave radiation is inherited from Wang and Liang \(2009\). We first compared the flux-tower-derived night-time LST estimates between 1:00-1:30 A.M. and 1:30-2:00 A.M.. As shown by Fig.A4-\(a\), the very slight RMSD of 0.72 K suggests that LST is generally stable between 1:00 and 2:00 A.M. at night. In Fig.A4-\(b\), we also found marginal bias and RMSD within 1 K between average flux-tower-derived LST of 1:00- 2:00 A.M. and the corresponding 0-cm ground temperature at close meteorological sites \(within 1 km and at 2:00 A.M.\).](#)

[In Fig.A4-\(c\) we demonstrate time series for monthly average NDVI \(derived as in Section 2.2.1\) at the 1-km pixels containing each of the four sites from 2003-2019. Clearly, there are very rare cases with NDVI values exceeding 0.5, corroborating the “open environmental conditions” met by the meteorological stations. In view of above, it is feasible for our study to have used the 0-cm ground temperature at pixels of such moderate to low vegetation covers as the evaluation benchmark of the satellite-derived thermal infrared LST.](#)

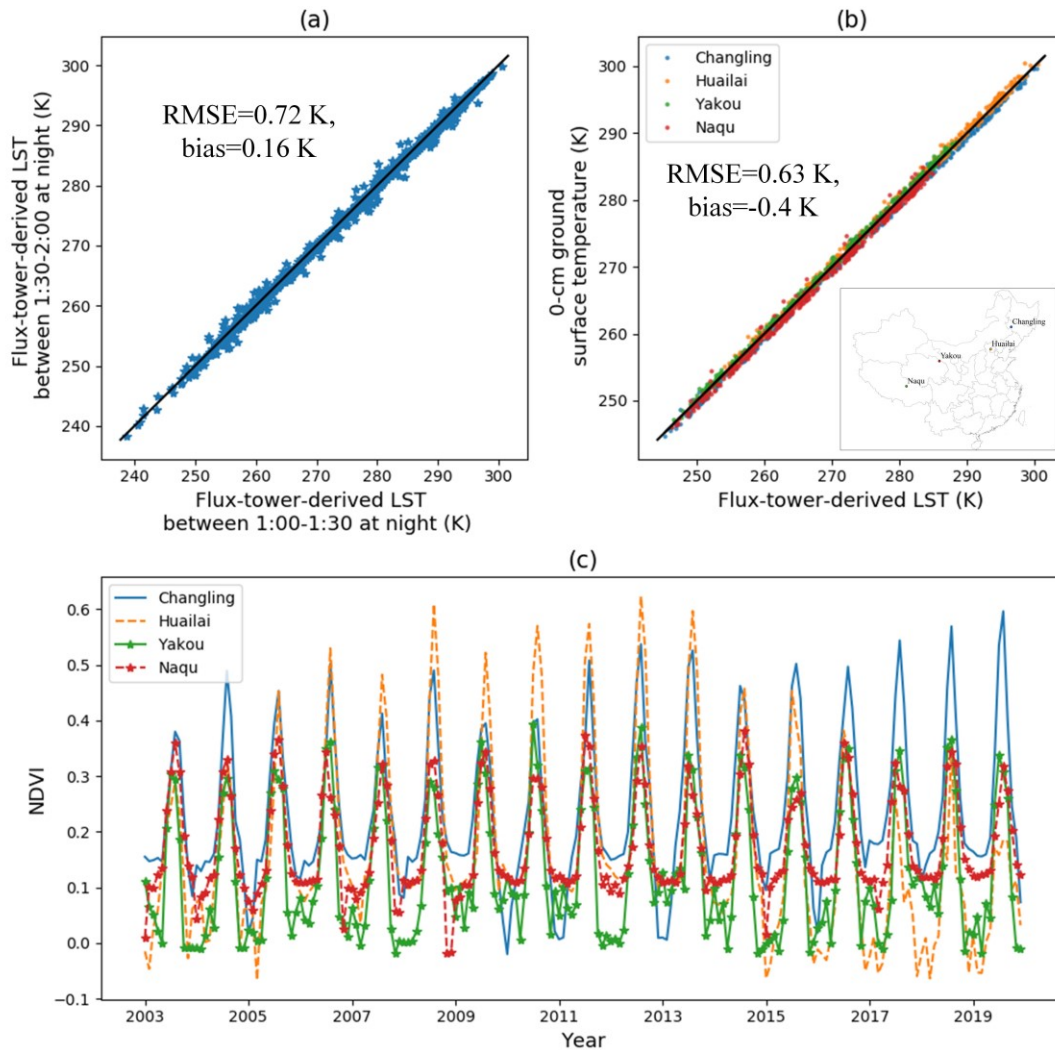


Fig. A4 (a) Comparison of LST between 1:00-1:30 A.M. and 1:30-2:00 A.M. for the four selected flux towers. (b) Comparison of flux-tower-derived LST averaged for 1:00-2:00 A.M. at the four towers and corresponding night-time 0-cm ground temperature at proximal meteorological stations. The inset map shows the location of the four flux towers. (3) Monthly NDVI time series for 1-km pixels containing each of the four flux towers.

Author contributions

Peilin Song and Yongqiang Zhang designed the research and developed the whole methodological framework; Peilin Song and Yongqiang Zhang supervised the processing line of the 1-km SSM product; Jianping Guo and Bingtong provided in situ

soil moisture data for validation; Peilin Song wrote the original draft of the manuscript; Yongqiang Zhang, Jiancheng Shi, and Tianjie Zhao revised the manuscript.

Competing interests

The authors declare that they have no conflict of interest.

Data availability

The published SSM dataset is available under the Creative Commons Attribution 4.0 International License at the following link: <http://dx.doi.org/10.11888/Hydro.tpd.271762> (Song and Zhang, 2021a). This dataset covers all of China's terrestrial area at a daily revisit frequency (about 1:30 A.M. at local time) and a 1km spatial resolution from January 2003 to October 2011 and from July 2012 to December 2019.

Acknowledgement

The authors would like to thank the National Aeronautics and Space Administration (NASA) for providing all MODIS and DEM data sets free of charge.

Financial support

This study was jointly supported by the National Natural Science Foundation of China (Grant No. 42001304), the Open Fund of State Key Laboratory of Remote Sensing Science (Grant No. OFSLRSS202117), CAS Pioneer Talents Program, CAS-

CSIRO International Cooperation Program, and the International Partnership Program
of Chinese Academy of Sciences (Grant No. 183311KYSB20200015).

References

- Albergel, C., de Rosnay, P., Gruhier, C., Munoz-Sabater, J., Hasenauer, S., Isaksen, L., . . . Wagner, W.: Evaluation of remotely sensed and modelled soil moisture products using global ground-based in situ observations, *Remote Sens. Environ.*, 118, 215-226, 10.1016/j.rse.2011.11.017, 2012.
- Brunsdon, C., Fotheringham, A. S., and Charlton, M. E.: Geographically weighted regression: A method for exploring spatial nonstationarity, *Geogr. Anal.*, 28, 281-298, 1996.
- Busch, F. A., Niemann, J. D., and Coleman, M.: Evaluation of an empirical orthogonal function-based method to downscale soil moisture patterns based on topographical attributes, *Hydrological Processes*, 26, 2696-2709, 2012.
- Carlson, T. N., Gillies, R. R., and Perry, E. M.: A method to make use of thermal infrared temperature and NDVI measurements to infer surface soil water content and fractional vegetation cover, *Remote sensing reviews*, 9, 161-173, 1994.
- Champagne, C., McNairn, H., and Berg, A. A.: Monitoring agricultural soil moisture extremes in Canada using passive microwave remote sensing, *Remote Sens. Environ.*, 115, 2434-2444, 2011.
- Chauhan, N. S., Miller, S., and Ardanuy, P.: Spaceborne soil moisture estimation at high resolution: a microwave-optical/IR synergistic approach, *Int. J. Remote Sens.*, 24, 4599-4622, <http://doi.org/10.1080/0143116031000156837>, 2003.
- Chen, Y., Yuan, H., Yang, Y., and Sun, R.: Sub-daily soil moisture estimate using dynamic Bayesian model averaging, *J. Hydrol.*, 590, 125445, <https://doi.org/10.1016/j.jhydrol.2020.125445>, 2020.
- Choi, M. and Hur, Y.: A microwave-optical/infrared disaggregation for improving spatial representation of soil moisture using AMSR-E and MODIS products, *Remote Sens. Environ.*, 124, 259-269, <http://doi.org/10.1016/j.rse.2012.05.009>, 2012.
- Das, N., Entekhabi, D., Dunbar, R. S., Kim, S., Yueh, S., Colliander, A., . . . Cosh, M.: SMAP/Sentinel-1 L2 Radiometer/Radar 30-Second Scene 3 km EASE-Grid Soil Moisture, Version 3 [dataset], <https://doi.org/10.5067/ASB0EQO2LYJV>, 2020.
- Das, N. N., Entekhabi, D., Dunbar, R. S., Chaubell, M. J., Colliander, A., Yueh, S., . . . Thibault, M.: The SMAP and Copernicus Sentinel 1A/B microwave active-passive high resolution surface soil moisture product, *Remote Sens. Environ.*, 233, 111380, <https://doi.org/10.1016/j.rse.2019.111380>, 2019.
- den Besten, N., Steele-Dunne, S., de Jeu, R., and van der Zaag, P.: Towards Monitoring Waterlogging with Remote Sensing for Sustainable Irrigated Agriculture, *Remote Sens.*, 13, 2021.

919 Dorigo, W., Himmelbauer, I., Aberer, D., Schremmer, L., Petrakovic, I., Zappa, L., . . . Sabia, R.: The International Soil Moisture
920 Network: serving Earth system science for over a decade, *Hydrol. Earth Syst. Sci.*, 25, 5749-5804, 10.5194/hess-25-5749-
921 2021, 2021.

922 Dowling, T. P. F., Song, P., Jong, M. C. D., Merbold, L., Wooster, M. J., Huang, J., and Zhang, Y.: An Improved Cloud Gap-
923 Filling Method for Longwave Infrared Land Surface Temperatures through Introducing Passive Microwave Techniques,
924 *Remote Sens.*, 13, 3522, 2021.

925 Du, J. Y., Kimball, J. S., and Jones, L. A.: Passive microwave remote sensing of soil moisture based on dynamic vegetation
926 scattering properties for AMSR-E, *IEEE Trans. Geosci. Remote Sens.*, 54, 597-608, 2016.

927 Duan, S. and Li, Z.: Spatial Downscaling of MODIS Land Surface Temperatures Using Geographically Weighted Regression:
928 Case Study in Northern China, *IEEE Trans. Geosci. Remote Sens.*, 54, 6458-6469,
929 <http://doi.org/10.1109/TGRS.2016.2585198>, 2016.

930 Entekhabi, D., Reichle, R. H., Koster, R. D., and Crow, W. T.: Performance Metrics for Soil Moisture Retrievals and Application
931 Requirements, *J. Hydrometeorol.*, 11, 832-840, 10.1175/2010jhm1223.1, 2010a.

932 Entekhabi, D., Das, N., Kim, S., Jagdhuber, T., Piles, M., Yueh, S., . . . Martínez-Fernández, J.: High-Resolution Enhanced Product
933 based on SMAP Active-Passive Approach and Sentinel 1A Radar Data, *AGU Fall Meeting Abstracts*, H24C-08,

934 Entekhabi, D., Njoku, E. G., O'Neill, P. E., Kellogg, K. H., Crow, W. T., Edelstein, W. N., . . . Van Zyl, J.: The Soil Moisture
935 Active Passive (SMAP) Mission, *Proc. IEEE*, 98, 704-716, <http://doi.org/10.1109/JPROC.2010.2043918>, 2010b.

936 Fang, B. and Lakshmi, V.: Passive Microwave Soil Moisture Downscaling Using Vegetation and Surface Temperatures, *Vadose*
937 *Zone J*, 12, 1712-1717, 2013.

938 Fang, B., Lakshmi, V., Bindlish, R., and Jackson, T.: AMSR2 Soil Moisture Downscaling Using Temperature and Vegetation Data,
939 *Remote Sens.*, 10, 2018.

940 Fang, B., Lakshmi, V., Bindlish, R., Jackson, T. J., Cosh, M., and Basara, J.: Passive Microwave Soil Moisture Downscaling Using
941 Vegetation Index and Skin Surface Temperature, 2013.

942 Fujii, H., Koike, T., and Imaoka, K.: Improvement of the AMSR-E Algorithm for Soil Moisture Estimation by Introducing a
943 Fractional Vegetation Coverage Dataset Derived from MODIS Data, *Journal of the Remote Sensing Society of Japan*, 29,
944 282-292, 2009.

945 Im, J., Park, S., Rhee, J., Baik, J., and Choi, M.: Downscaling of AMSR-E soil moisture with MODIS products using machine
946 learning approaches, *Environ Earth Sci*, 75, 1-19, <http://doi.org/10.1007/s12665-016-5917-6>, 2016.

947 Ines, A. V. M., Das, N. N., Hansen, J. W., and Njoku, E. G.: Assimilation of remotely sensed soil moisture and vegetation with a
948 crop simulation model for maize yield prediction, *Remote Sens. Environ.*, 138, 149-164, 10.1016/j.rse.2013.07.018, 2013.

-
- Jeffrey, P., Walker, Paul, R., and Houser: A methodology for initializing soil moisture in a global climate model: Assimilation of near-surface soil moisture observations, *Journal of Geophysical Research Atmospheres*, 2001.
- Jiménez, C., Prigent, C., Ermida, S. L., and Moncet, J. L.: Inversion of AMSR-E observations for land surface temperature estimation: 1. Methodology and evaluation with station temperature, *Journal of Geophysical Research: Atmospheres*, 2017.
- Jing, Z. and Zhang, X.: A soil moisture assimilation scheme using satellite-retrieved skin temperature in meso-scale weather forecast model, *Atmos Res*, 95, 333-352, 2010.
- Jones, L. A., Kimball, J. S., Podest, E., McDonald, K. C., Chan, S. K., and Njoku, E. G.: A method for deriving land surface moisture, vegetation optical depth, and open water fraction from AMSR-E, *IEEE IGARSS 2009*, Cape Town, South Africa, 2009, III-916-III-919, <http://doi.org/10.1109/IGARSS.2009.5417921>,
- Jung, M., Reichstein, M., Ciais, P., Seneviratne, S. I., Sheffield, J., Goulden, M. L., . . . Zhang, K.: Recent decline in the global land evapotranspiration trend due to limited moisture supply, *Nature*, 467, 951-954, 10.1038/nature09396, 2010.
- Kim, J. and Hogue, T. S.: Improving spatial soil moisture representation through integration of AMSR-E and MODIS products, *IEEE Trans. Geosci. Remote Sens*, 50, 446-460, <http://doi.org/10.1109/TGRS.2011.2161318>, 2012.
- Koike, T., Nakamura, Y., Kaihotsu, I., Davva, G., Matsuura, N., Tamagawa, K., and Fujii, H.: Development of an Advanced Microwave Scanning Radiometer (AMSR-E) algorithm of soil moisture and vegetation water content (written in Japanese), *Annual Journal of Hydraulic Engineering*, 48, 217-222 2004.
- Komatsu, T. S.: Toward a Robust Phenomenological Expression of Evaporation Efficiency for Unsaturated Soil Surfaces, *Journal of Applied Meteorology*, 42, 1330-1334, 10.1175/1520-0450(2003)042<1330:Tarpeo>2.0.Co;2, 2003.
- Kong, D., Zhang, Y., Gu, X., and Wang, D.: A robust method for reconstructing global MODIS EVI time series on the Google Earth Engine, *Isprs J Photogramm*, 155, 13-24, 2019.
- Koster, R. D., Mahanama, S., Livneh, B., Lettenmaier, D. P., and Reichle, R. H.: Skill in streamflow forecasts derived from large-scale estimates of soil moisture and snow, *Nature Geoscience*, 3, 613-616, 2010.
- Malbêteau, Y., Merlin, O., Molero, B., Rüdiger, C., and Bacon, S.: DisPATCh as a tool to evaluate coarse-scale remotely sensed soil moisture using localized in situ measurements: Application to SMOS and AMSR-E data in Southeastern Australia, *Int J Appl Earth Obs*, 45, 221-234, <https://doi.org/10.1016/j.jag.2015.10.002>, 2016.
- Meesters, A. G. C. A., De Jeu, R. A. M., and Owe, M.: Analytical derivation of the vegetation optical depth from the microwave polarization difference index, *IEEE Geosci. Remote Sens. Lett.*, 2, 121-123, 2005.
- Mendoza, P. A., Mizukami, N., Ikeda, K., Clark, M. P., Gutmann, E. D., Arnold, J. R., . . . Rajagopalan, B.: Effects of different regional climate model resolution and forcing scales on projected hydrologic changes, *J. Hydrol.*, 541, 1003-1019, <https://doi.org/10.1016/j.jhydrol.2016.08.010>, 2016.

-
- Meng, X. J., Mao, K. B. A., Meng, F., Shi, J. C., Zeng, J. Y., Shen, X. Y., . . . Guo, Z. H.: A fine-resolution soil moisture dataset for China in 2002-2018, *Earth System Science Data*, 13, 3239-3261, 10.5194/essd-13-3239-2021, 2021.
- Merlin, O., Al Bitar, A., Walker, J. P., and Kerr, Y.: An improved algorithm for disaggregating microwave-derived soil moisture based on red, near-infrared and thermal-infrared data, *Remote Sens. Environ.*, 114, 2305-2316, <http://doi.org/10.1016/j.rse.2010.05.007>, 2010.
- Merlin, O., Walker, J. P., Chehbouni, A., and Kerr, Y.: Towards deterministic downscaling of SMOS soil moisture using MODIS derived soil evaporative efficiency, *Remote Sens. Environ.*, 112, 3935-3946, <http://doi.org/10.1016/j.rse.2008.06.012>, 2008.
- Merlin, O., Chehbouni, A. G., Kerr, Y. H., Njoku, E. G., and Entekhabi, D.: A combined modeling and multipectral/multiresolution remote sensing approach for disaggregation of surface soil moisture: Application to SMOS configuration, *IEEE Trans. Geosci. Remote Sens.*, 43, 2036-2050, <http://doi.org/10.1109/TGRS.2005.853192>, 2005.
- Merlin, O., Escorihuela, M. J., Mayoral, M. A., Hagolle, O., Al Bitar, A., and Kerr, Y.: Self-calibrated evaporation-based disaggregation of SMOS soil moisture: An evaluation study at 3 km and 100 m resolution in Catalunya, Spain, *Remote Sens. Environ.*, 130, 25-38, 10.1016/j.rse.2012.11.008, 2013.
- Merlin, O., Malbeteau, Y., Notfi, Y., Bacon, S., Er-Raki, S., Khabba, S., and Jarlan, L.: Performance Metrics for Soil Moisture Downscaling Methods: Application to DISPATCH Data in Central Morocco, *Remote Sens.*, 7, 3783-3807, <http://doi.org/10.3390/rs70403783>, 2015.
- Molero, B., Merlin, O., Malbêteau, Y., Al Bitar, A., Cabot, F., Stefan, V., . . . Jackson, T. J.: SMOS disaggregated soil moisture product at 1km resolution: Processor overview and first validation results, *Remote Sens. Environ.*, 180, 361-376, <http://doi.org/10.1016/j.rse.2016.02.045>, 2016.
- Montaldo, N., Albertson, J. D., Mancini, M., and Kiely, G.: Robust simulation of root zone soil moisture with assimilation of surface soil moisture data, *Water Resour Res.*, 37, 2889-2900, 10.1029/2000WR000209, 2001.
- Owe, M., de Jeu, R., and Walker, J.: A methodology for surface soil moisture and vegetation optical depth retrieval using the microwave polarization difference index, *IEEE Trans. Geosci. Remote Sens.*, 39, 1643-1654, 2001.
- Pan, H., Chen, Z., Wit, A. D., and Ren, J.: Joint Assimilation of Leaf Area Index and Soil Moisture from Sentinel-1 and Sentinel-2 Data into the WOFOST Model for Winter Wheat Yield Estimation, *Sensors (Basel, Switzerland)*, 19, 2019.
- Peng, J., Loew, A., Zhang, S. Q., Wang, J., and Niesel, J.: Spatial downscaling of satellite soil moisture data using a vegetation temperature condition index, *IEEE Trans. Geosci. Remote Sens.*, 54, 558-566, <http://doi.org/10.1109/TGRS.2015.2462074>, 2016.

-
- Piles, M., Entekhabi, D., and Camps, A.: A Change Detection Algorithm for Retrieving High-Resolution Soil Moisture From SMAP Radar and Radiometer Observations, *IEEE Trans. Geosci. Remote Sens.*, 47, 4125-4131, 10.1109/TGRS.2009.2022088, 2009.
- Sabaghy, S., Walker, J. P., Renzullo, L. J., Akbar, R., Chan, S., Chaubell, J., . . . Yueh, S.: Comprehensive analysis of alternative downscaled soil moisture products, *Remote Sens. Environ.*, 239, 111586, <https://doi.org/10.1016/j.rse.2019.111586>, 2020.
- Sanchez-Ruiz, S., Piles, M., Sanchez, N., Martinez-Fernandez, J., Vall-Ilossera, M., and Camps, A.: Combining SMOS with visible and near/shortwave/thermal infrared satellite data for high resolution soil moisture estimates, *J. Hydrol.*, 516, 273-283, 10.1016/j.jhydrol.2013.12.047, 2014.
- Scaini, A., Sanchez, N., Vicente-Serrano, S. M., and Martinez-Fernandez, J.: SMOS-derived soil moisture anomalies and drought indices: a comparative analysis using in situ measurements, *Hydrological Processes*, 29, 373-383, 10.1002/hyp.10150, 2015.
- Song, P. and Zhang, Y.: Daily all weather surface soil moisture data set with 1 km resolution in China (2003-2019), National Tibetan Plateau Data Center [dataset], 10.11888/Hydro.tpd.271762, 2021a.
- Song, P. and Zhang, Y.: An improved non-linear inter-calibration method on different radiometers for enhancing coverage of daily LST estimates in low latitudes, *Remote Sens. Environ.*, 264, 112626, <https://doi.org/10.1016/j.rse.2021.112626>, 2021b.
- Song, P., Huang, J., and Mansaray, L. R.: An improved surface soil moisture downscaling approach over cloudy areas based on geographically weighted regression, *Agr Forest Meteorol.*, 275, 146-158, 10.1016/j.agrformet.2019.05.022, 2019a.
- Song, P., Zhang, Y., and Tian, J.: Improving Surface Soil Moisture Estimates in Humid Regions by an Enhanced Remote Sensing Technique, *Geophys Res Lett.*, 48, e2020GL091459, <https://doi.org/10.1029/2020GL091459>, 2021.
- Song, P., Mansaray, L. R., Huang, J., and Huang, W.: Mapping paddy rice agriculture over China using AMSR-E time series data, *Isprs J Photogramm.*, 144, 469-482, 10.1016/j.isprs.2018.08.015, 2018.
- Song, P., Huang, J., Mansaray, L. R., Wen, H., Wu, H., Liu, Z., and Wang, X.: An Improved Soil Moisture Retrieval Algorithm Based on the Land Parameter Retrieval Model for Water-Land Mixed Pixels Using AMSR-E Data, *IEEE Trans. Geosci. Remote Sens.*, 1-15, 10.1109/TGRS.2019.2915346, 2019b.
- Sui, D. Z.: Tobler's First Law of Geography: A Big Idea for a Small World?, *Annals of the Association of American Geographers*, 94, 269-277, <https://doi.org/10.1111/j.1467-8306.2004.09402003.x>, 2004.
- Vergopolan, N., Xiong, S. T., Estes, L., Wanders, N., Chaney, N. W., Wood, E. F., . . . Sheffield, J.: Field-scale soil moisture bridges the spatial-scale gap between drought monitoring and agricultural yields, *Hydrol. Earth Syst. Sci.*, 25, 1827-1847, 2021.

-
- Verstraeten, W. W., Veroustraete, F., van der Sande, C. J., Grootaers, I., and Feyen, J.: Soil moisture retrieval using thermal inertia, determined with visible and thermal spaceborne data, validated for European forests, *Remote Sens. Environ.*, 101, 299-314, 2006.
- Wang, K. and Liang, S.: Evaluation of ASTER and MODIS land surface temperature and emissivity products using long-term surface longwave radiation observations at SURFRAD sites, *Remote Sens. Environ.*, 113, 1556-1565, <https://doi.org/10.1016/j.rse.2009.03.009>, 2009.
- Wang, L. and Qu, J. J.: NMDI: A normalized multi-band drought index for monitoring soil and vegetation moisture with satellite remote sensing, *Geophys Res Lett*, 34, L20405, 10.1029/2007GL031021, 2007.
- Wei, Z., Meng, Y., Zhang, W., Peng, J., and Meng, L.: Downscaling SMAP soil moisture estimation with gradient boosting decision tree regression over the Tibetan Plateau, *Remote Sens. Environ.*, 225, 30-44, 2019.
- Wu, D., Liang, H., Cao, T., Yang, D., Zhou, W., and Wu, X.: Construction of operation monitoring system of automatic soil moisture observation network in China, *Meteorological Science and Technology*, 42, 278-282, 2014
- Yang, G., Sun, W. W., Shen, H. F., Meng, X. C., and Li, J. L.: An Integrated Method for Reconstructing Daily MODIS Land Surface Temperature Data, *IEEE J. Sel. Top. Appl. Earth Observ. Remote Sens.*, 12, 1026-1040, 2019.
- Yao, P., Lu, H., Shi, J., Zhao, T., Yang, K., Cosh, M. H., . . . Entekhabi, D.: A long term global daily soil moisture dataset derived from AMSR-E and AMSR2 (2002–2019), *Scientific Data*, 8, 143, 10.1038/s41597-021-00925-8, 2021.
- Zeng, Y., Feng, Z., and Xiang, N.: Assessment of soil moisture using Landsat ETM+ temperature/vegetation index in semiarid environment, *IEEE International Geoscience & Remote Sensing Symposium*, Piscataway NJ, 2004, 4306-4309 vol.4306, 10.1109/IGARSS.2004.1370089,
- Zhang, J., Zhou, Z., Yao, F., Yang, L., and Hao, C.: Validating the Modified Perpendicular Drought Index in the North China Region Using In Situ Soil Moisture Measurement, *IEEE Geoscience & Remote Sensing Letters*, 12, 542-546, 2014.
- Zhang, Y., Kong, D., Gan, R., Chiew, F. H. S., Mcvicar, T. R., Zhang, Q., and Yang, Y.: Coupled estimation of 500 m and 8-day resolution global evapotranspiration and gross primary production in 2002-2017, *Remote Sens. Environ.*, 222, 165-182, 2019.
- Zhang, Y. Q., Chiew, F. H. S., Liu, C. M., Tang, Q. H., Xia, J., Tian, J., . . . Li, C. C.: Can Remotely Sensed Actual Evapotranspiration Facilitate Hydrological Prediction in Ungauged Regions Without Runoff Calibration?, *Water Resour Res*, 56, 2020.
- Zheng, J. Y., Lu, H. S., Crow, W. T., Zhao, T. J., Merlin, O., Rodriguez-Fernandez, N., . . . Gou, Q. Q.: Soil moisture downscaling using multiple modes of the DISPATCH algorithm in a semi-humid/humid region, *Int J Appl Earth Obs*, 104, 10.1016/j.jag.2021.102530, 2021.

1064 Zhou, S., Williams, A. P., Lintner, B., Berg, A. M., and Gentine, P.: Soil moisture–atmosphere feedbacks mitigate declining water
1065 availability in drylands, *Nature Climate Change*, 11, 2021.
1066 Zhu, Z. and Shi, C.: Simulation and Evaluation of CLDAS and GLDAS Soil Moisture Data in China (written in Chinese), *Science*
1067 *Technology and Engineering*, 32, 138-144, 2014.
1068